

GLHF: General Learned Evolutionary Algorithm Via Hyper Functions

Xiaobin Li¹ Kai Wu¹ Yujian Betterest Li¹ Xiaoyu Zhang² Handing Wang¹ Jing Liu³

Abstract

Pretrained Optimization Models (POMs) leverage knowledge gained from optimizing various tasks, providing efficient solutions for new optimization challenges through direct usage or fine-tuning. Despite the inefficiencies and limited generalization abilities observed in current POMs, our proposed model, the general pre-trained optimization model (GPOM), addresses these shortcomings. GPOM constructs a population-based pretrained Black-Box Optimization (BBO) model tailored for continuous optimization. Evaluation on the BBOB benchmark and two robot control tasks demonstrates that GPOM outperforms other pretrained BBO models significantly, especially for high-dimensional tasks. Its direct optimization performance exceeds that of state-of-the-art evolutionary algorithms and POMs. Furthermore, GPOM exhibits robust generalization capabilities across diverse task distributions, dimensions, population sizes, and optimization horizons.

1. Introduction

A Black Box Optimization (BBO) algorithm is designed to address black box optimization problems, including tasks like hyperparameter optimization (HPO) (Hutter et al., 2019), neuroevolution (Such et al., 2017), neural architecture search (NAS) (Ye et al., 2021), multi-objective optimization (Deb et al., 2002), and multi-task optimization (Bali et al., 2019). In these scenarios, the algorithm can evaluate $f(\mathbf{x})$ for any solution \mathbf{x} ; however, access to additional information about f , such as the Hessian and gradients, is unavailable.

In light of the "No Free Lunch Theorem" (Wolpert &

^{*}Equal contribution ¹School of Artificial Intelligence, Xidian University, Xi'an 710071, China ²School of Cyber Engineering, Xidian University, Xi'an 710071, China ³Guangzhou Institute of Technology, Xidian University, Xidian University, Guangzhou 510555, China. Correspondence to: Kai Wu <kwu@xidian.edu.cn>.

Proceedings of the 41st International Conference on Machine Learning, Vienna, Austria. PMLR 235, 2024. Copyright 2024 by the author(s).

Macready, 1997), it is recognized that no single algorithm can universally excel across all scenarios. Therefore, addressing diverse BBO problems necessitates the tailored design of specific algorithms to achieve satisfactory performance. Crafting these algorithms typically demands substantial expertise. Presently, researchers heavily rely on manual engineering for BBO algorithm design (Liu et al., 2023b). In this manual design paradigm, the process involves "trial and error" guided by past "optimization experience" (Gämperle et al., 2002; Ronkkonen et al., 2005; Tvrđik, 2006). However, this approach is cumbersome, and the subjective nature of "optimization experience" introduces variability across individuals, posing a risk of domain overfitting. Furthermore, the resulting optimization strategy tends to exhibit limited generalization ability when applied to new tasks.

In recent years, pretrained optimization models, a pivotal facet of AutoML (Hutter et al., 2019), have shown promise in overcoming the limitations of human-designed BBO algorithms. These models, general-purpose optimizers learning from the experience of optimizing multiple tasks, can be applied directly or fine-tuned to efficiently address new optimization tasks. (Chen et al., 2022; Krishnamoorthy et al., 2022; 2023) employ Transformer or diffusion models to pre-train model-based optimizers using offline datasets. While effective, these methods primarily fit optimization trajectories of other BBO algorithms to a specific task, potentially requiring retraining for new tasks, limiting their generalizability. Subsequently, (Lange et al., 2023b) introduced two bilevel optimization frameworks for meta-learning evolution strategy (ES) and genetic algorithm (GA). Furthermore, they still grapple with the curse of dimensionality (Chen et al., 2015) attributed to nonconvex objectives in the outer loop and the constrained search strategy derived from optimization trajectories.

To address the inefficiencies and low generality of existing methods, we introduce the General Pretrained Optimization Model, called GPOM. GPOM constructs a population-based pretrained BBO model for continuous optimization. Leveraging multiple individuals, population-based optimizers gain a better understanding of the fitness landscape. Consequently, employing a population-based Differential Evolution (DE) (Storn & Price, 1997; Thangaraj et al., 2009) mechanism with crossover, mutation, and selection opera-

tors, we design Learnable Mutation Module (LMM), Learnable Crossover Module (LCM), and Selection Module for GPOM. These modules equip GPOM with advanced optimization capabilities. Pretraining GPOM on a set of training functions ensures good convergence and generalization. Drawing inspiration from (Finn et al., 2017), we introduce an end-to-end gradient-based training method for GPOM, termed *MetaGBT* (Meta Gradient-Based Training), ensuring stable and rapid training for GPOM.

We evaluate the performance and generalization capabilities of GPOM on BBOB (Finck et al., 2010) and two robot control tasks (Brockman et al., 2016). Notably, GPOM exhibits superior optimization capabilities compared to other pretrained BBO models, outperforming them significantly. Even in the context of high-dimensional tasks (4149 dimensions), GPOM excels in directly optimizing new tasks, surpassing state-of-the-art population-based optimizers. Furthermore, GPOM showcases adaptive revision of its optimization strategy (LMM and LCM) based on the current population status, striking a commendable balance between exploration and exploitation. An in-depth analysis reveals that training GPOM on simpler tasks yields better results. Our contributions can be summarized as follows:

- GPOM stands out as the current leading pretrained BBO model, demonstrating a substantial performance advantage over other models. Its effectiveness extends to direct optimization of new tasks, surpassing state-of-the-art population-based optimizers, even in high-dimensional scenarios.
- GPOM exhibits remarkable generalization across diverse task distributions, dimensions, population sizes, and optimization horizons, addressing challenges faced by existing POMs.

2. Related Work

Heuristic Population-based BBO Algorithms Numerous metaheuristic population-based algorithms, such as genetic algorithms (Holland, 1992), evolution strategies (Hansen & Ostermeier, 2001; Hansen et al., 2003; Ros & Hansen, 2008), particle swarm optimization (Kennedy & Eberhart, 1995; Gong et al., 2015), and differential evolution (Storn & Price, 1997; Stanovov et al., 2022), have been devised to address optimization problems. Notably, CMA-ES (Hansen, 2016) and L-SHADE (Tanabe & Fukunaga, 2014) stand out as state-of-the-art methods for BBO. However, these approaches rely on manually designed components, exhibiting inefficiency and fragility when confronted with new tasks. In contrast, the proposed GPOM can autonomously acquire optimization strategies from problem instances, mitigating the aforementioned limitations.

Pretrained Population-based BBO Algorithms Pre-training BBO algorithms can be categorized into two types within the meta-learning framework. The first type frames meta-learning BBO algorithms as a bi-level optimization problem (Liu et al., 2022). For instance, (Gomes et al., 2021) leverages meta-learning to infer population-based black-box optimizers that automatically adapt to specific task classes. LES (Lange et al., 2023b) designs a self-attention-based search strategy for discovering effective update rules for evolution strategies through meta-learning. Subsequent works like LGA (Lange et al., 2023a) utilize this framework to discover the update rules of Gaussian genetic algorithms via Open-ES (Zhang et al., 2017). The second type models the meta-learning of a BBO algorithm as a reinforcement learning problem. (Shala et al., 2020) meta-learn a policy that adjusts the mutation step-size parameters of CMA-ES (Hansen, 2016). Category one faces the curse of dimensionality, where an escalating number of optimization strategy parameters leads to skyrocketing training difficulty, impeding the development of intricate strategies. In contrast, category two, which models meta-learning optimizers as reinforcement learning tasks, grapples with training instability. GPOM, employing a gradient-based end-to-end training approach, successfully bypasses the curse of dimensionality, ensuring stable training.

LLM for Optimization In line with POMs, various optimization approaches leveraging Large Language Models (LLMs) have emerged to address diverse problem domains, including NP-hard problems (Romera-Paredes et al., 2023; Meyerson et al., 2023), algorithm evolution (Liu et al., 2023a; Yang et al., 2023; Lehman et al., 2023), reward design (Ma et al., 2023), and Neural Architecture Search (NAS) (Chen et al., 2023; Nasir et al., 2023). Notably, LLMs play a role in sampling new solutions. However, their optimization strategies depend on externally introduced natural selection mechanisms and are less effective in numerical optimization scenarios. These methods lack the universal applicability as pretrained BBO models due to a deficiency in generating capabilities across tasks.

3. GPOM

3.1. Problem Definition

A black-box optimization problem can be transformed as a minimization problem, as shown in Eq. (1), and constraints may exist for corresponding solutions:

$$\min_{\mathbf{x}} f(\mathbf{x}), \text{s.t. } x_i \in [l_i, u_i] \quad (1)$$

where $\mathbf{x} = (x_1, x_2, \dots, x_d)$ represents the solution of optimization problem f , the lower and upper bounds $\mathbf{l} = (l_1, l_2, \dots, l_d)$ and $\mathbf{u} = (u_1, u_2, \dots, u_d)$, and d is the dimension of \mathbf{x} . A population consists of n individuals, de-

noted as $\mathbf{X} = \{\mathbf{x}_1, \mathbf{x}_2, \dots, \mathbf{x}_n\}$. In this paper, \mathbf{X} is also treated as $\mathbf{X} = [\mathbf{x}_1, \mathbf{x}_2, \dots, \mathbf{x}_n]^T$ to support matrix operations. We feed GPOM an initial random population \mathbf{X}^0 at step 0, specify the evolution generation T for it, and hope that it can generate a population \mathbf{X}^T close to the global optimum at step T , as shown in Eq. (2).

$$\mathbf{X}^T = GPOM(\mathbf{X}^0, T|\theta) \quad (2)$$

$\theta \in \Omega$ is the parameters of GPOM, where Ω stands for the strategy space. The goal of training GPOM is to find an optimal θ in Ω .

3.2. Parameterization of DE

DE (Storn & Price, 1997; Thangaraj et al., 2009) constitutes a pivotal algorithmic family within BBO, celebrated for its commendable attributes like rapid convergence and robustness (Das et al., 2016; Neri & Tirronen, 2010).

Mutation Strategy Generalization Illustratively, considering the classic DE mutation strategy, DE/rand/1, it is defined as $\mathbf{v}_i^t = \mathbf{x}_{r1}^t + F \cdot (\mathbf{x}_{r2}^t - \mathbf{x}_{r3}^t)$ (refer to Appendix A for additional mutation strategies). Here, the integer index $r1$ (likewise, $r2$ and $r3$) is randomly chosen from the range $[0, N]$ and F is constant. The generalized formulation of the mutation strategy is presented as:

$$\mathbf{v}_i^t = \sum_j^N w_{i,j} \mathbf{x}_j \quad (\forall w_{i,j} \in \mathbb{R}) \quad (3)$$

Further, we organize the mutation strategy into a matrix form, as shown in Eq. (4).

$$\mathbf{V}^t = \mathbf{S}^t \times \mathbf{X}^t \quad (4)$$

$\mathbf{X}^t = [\mathbf{x}_1^t, \mathbf{x}_2^t, \dots, \mathbf{x}_N^t]$, ($\mathbf{X}^t \in \mathbb{R}^{N \times d}$) is the population in generation t and \mathbf{S}^t is the matrix shown as follows:

$$\mathbf{S}^t = \begin{bmatrix} s_{1,1}^t & \dots & s_{1,N}^t \\ \vdots & \ddots & \vdots \\ s_{N,1}^t & \dots & s_{N,N}^t \end{bmatrix} \quad (5)$$

\mathbf{S} evolves with each change in t , signifying a mutation strategy that adapts across generations. Consequently, it is imperative to devise a module that leverages information from the population at generation t to generate \mathbf{S}^t .

Crossover Strategy Generalization For each individual \mathbf{x}_i^t at step t , a crossover probability $cr_i^t \in [0, 1]$ is established. Consequently, the population's crossover strategy is encapsulated in the vector $\mathbf{cr}^t = (cr_1^t, cr_2^t, \dots, cr_N^t)$. The crossover operation, as depicted in Eq. (6), can be elucidated as follows:

$$\mathbf{u}_{i,k}^t = \begin{cases} \mathbf{v}_{i,k}^t, & \text{if } rand(0, 1) \leq cr_i^t \\ \mathbf{x}_{i,k}^t, & \text{otherwise} \end{cases} \quad \forall i \in [1, N] \quad (6)$$

The module design should facilitate the adaptive generation of \mathbf{cr}^t by leveraging population information. Executing the crossover operation with \mathbf{cr}^t yields $\mathbf{U}^t = [\mathbf{u}_1^t, \mathbf{u}_2^t, \dots, \mathbf{u}_N^t]$.

3.3. Design of GPOM

We design LMM and LCM to achieve the generation of mutation strategy (that is, generate \mathbf{S}^t) and crossover strategy (that is, generate \mathbf{cr}^t), respectively.

LMM The function of LMM is designed based on Multi-head self-attention (MSA) (Vaswani et al., 2017), as shown as follows:

$$\mathbf{S}^t = LMM(\mathbf{H}^t | \theta_1) \quad (7)$$

where $\theta_1 = \{\mathbf{W}_{m1}, \mathbf{W}_{m2}, \mathbf{W}_{m3}, \mathbf{b}_{m1}, \mathbf{b}_{m2}, \mathbf{b}_{m3}\}$ denotes the trainable parameters within LMM, while $\mathbf{H}^t = [\mathbf{h}_1^t, \mathbf{h}_2^t, \dots, \mathbf{h}_N^t]$ serves as LMM's input, encapsulating population information. Each \mathbf{h}_i^t incorporates details about \mathbf{x}_i^t , encompassing: 1) \hat{f}_i^t : the normalized fitness $f(\mathbf{x}_i^t)$ of \mathbf{x}_i^t ; 2) \hat{r}_i^t : the centralized ranking of \mathbf{x}_i^t . The method for calculating \hat{f}_i^t is:

$$\hat{f}_i^t = \frac{f(\mathbf{x}_i^t) - \mu^t}{\sigma^t} \quad (8)$$

where μ^t and σ^t denote the mean and standard deviation, respectively, of individual fitness values within the population at time t . We build \hat{r}_i^t as follows:

$$\hat{r}_i^t = \left(\frac{rank(\mathbf{x}_i^t, \mathbf{X}^t)}{N} - 0.5 \right) \times 2 \quad (9)$$

where $rank$ yields the ranking of \mathbf{x}_i^t within the population \mathbf{X}^t , with values ranging from 1 to N . Thus, LMM utilizes information on the relative fitness of individuals to dynamically generate the strategy $\hat{\mathbf{S}}^t$. \hat{r}_i^t serves as position encoding, explicitly offering the ranking information of individuals. Equation (10) details the computation of $\hat{\mathbf{S}}^t$.

$$\begin{aligned} \hat{\mathbf{H}}^t &= Tanh(\mathbf{H}^t \times \mathbf{W}_{m1} + \mathbf{b}_{m1}) \\ \mathbf{Q}^t &= Tanh(\hat{\mathbf{H}}^t \times \mathbf{W}_{m2} + \mathbf{b}_{m2}) \\ \mathbf{K}^t &= Tanh(\hat{\mathbf{H}}^t \times \mathbf{W}_{m3} + \mathbf{b}_{m3}) \\ \hat{\mathbf{S}}^t &= Tanh\left(\frac{\mathbf{Q}^t \times (\mathbf{K}^t)^T}{sqrt(d_m)}\right) \end{aligned} \quad (10)$$

where $Tanh$ is an activation function. $\mathbf{W}_{m1} \in \mathbb{R}^{2 \times d_m}$ and $\mathbf{W}_{m2}, \mathbf{W}_{m3} \in \mathbb{R}^{d_m \times d_m}$. $\mathbf{b}_{m1}, \mathbf{b}_{m2}$, and \mathbf{b}_{m3} are vector with dimension d_m . $\hat{\mathbf{H}}^t \in \mathbb{R}^{N \times d_m}$, $\mathbf{Q}^t, \mathbf{K}^t \in \mathbb{R}^{N \times d_m}$, and $\hat{\mathbf{S}}^t \in \mathbb{R}^{N \times N}$.

The topological structure of the population significantly influences their information exchange (Yu et al., 2021). When all individuals engage in information exchange, the algorithm's convergence may suffer, diversity could diminish, and susceptibility to local optima increases. To address this,

we introduce a *mask* operation during both training and testing phases, where the probability of setting each element in $\hat{\mathbf{S}}^t$ to 0 is r_{mask} . This operation enhances GPOM's ability to learn efficient and robust strategies, as validated in our experiments. Consequently, \mathbf{S}^t is derived using Eq. (11).

$$\mathbf{S}^t = \text{mask}(\hat{\mathbf{S}}^t | r_{mask}) \quad (11)$$

Finally, we get \mathbf{V}^t via Eq. (4).

LCM LCM is designed based on FFN (Vaswani et al., 2017), as shown in Eq. (12),

$$\mathbf{cr}^t = \text{LCM}(\mathbf{Z}^t | \theta_2) \quad (12)$$

where $\theta_2 = \{\mathbf{W}_{c1}, \mathbf{b}_{c1}, \mathbf{W}_{c2}, \mathbf{b}_{c2}, \tau\}$ is the parameter of LCM and $\mathbf{Z}^t \in \mathbb{R}^{N \times 4}$ is the population information used by LCM. Here, $\mathbf{Z}^t = [\mathbf{z}_1^t, \mathbf{z}_2^t, \dots, \mathbf{z}_N^t]$. \mathbf{z}_i^t represents the relevant information of individual \mathbf{x}_i^t and \mathbf{X}^t . For example, it can include the ranking information of \mathbf{x}_i^t , the fitness information of \mathbf{x}_i^t , the Euclidean distance between \mathbf{x}_i^t and \mathbf{V}_i^t , and the distribution information of individuals within the population (such as the fitness distribution, the distance between pairs of individuals), etc. In this paper, \mathbf{z}_i^t includes the following information as a case study: 1) \hat{f}_i^t : the normalized fitness $f(\mathbf{x}_i^t)$ of \mathbf{x}_i^t ; 2) \hat{r}_i^t : the centralized ranking of \mathbf{x}_i^t ; 3) $\hat{f}_{v_i}^t$: the normalized fitness $f(\mathbf{v}_i^t)$ of \mathbf{v}_i^t ; 4) $\hat{r}_{v_i}^t$: the centralized ranking of \mathbf{v}_i^t . Among them, $\hat{f}_{v_i}^t$ and $\hat{r}_{v_i}^t$ are calculated in the same way as \hat{f}_i^t and \hat{r}_i^t respectively. The detailed mechanism of LCM is shown in Eq. (13).

$$\begin{aligned} \mathbf{h}^t &= \text{Tanh}(\mathbf{Z}^t \times \mathbf{W}_{c1} + \mathbf{b}_{c1}) \\ \hat{\mathbf{h}}^t &= \text{layernorm}(\mathbf{h}^t | \tau) \\ \mathbf{cr}^t &= \text{Sigmoid}(\hat{\mathbf{h}}^t \times \mathbf{W}_{c2} + \mathbf{b}_{c2}) \end{aligned} \quad (13)$$

where the activation function *Sigmoid* maps inputs to the range $(0, 1)$. $\mathbf{W}_{c1} \in \mathbb{R}^{4 \times d_c}$, $\mathbf{W}_{c2} \in \mathbb{R}^{d_c \times 1}$, τ is the learnable parameters of *layernorm* (Xu et al., 2019). \mathbf{b}_{c1} and \mathbf{b}_{c2} are vectors with dimensions d_c and 1, respectively.

Although we derive \mathbf{cr}^t from Eq. (13) as in Eq. (6), the discrete nature of the crossover operator renders it non-differentiable, impeding gradient-based training of the *LCM* module. To address this limitation, we introduce the *gumbel-softmax* method (Jang et al., 2016), providing an efficient gradient estimator that replaces non-differentiable samples from a categorical distribution with differentiable samples from a novel Gumbel-Softmax distribution.

Eq. (14) shows how to perform crossover operations between \mathbf{x}_i^t and \mathbf{v}_i^t in *LCM* ($\forall i \in [1, N]$).

$$\begin{aligned} \mathbf{r}_i^t &= \text{rand}(d) \\ \mathbf{cv}_i^t &= \text{gumbel_softmax}(\text{cat}(\mathbf{r}_i^t, \text{tile}(\mathbf{cr}_i^t, d))) \\ \mathbf{u}_i^t &= \mathbf{cv}_{i,0}^t \cdot \mathbf{x}_i^t + \mathbf{cv}_{i,1}^t \cdot \mathbf{v}_i^t \\ \mathbf{U}^t &= [\mathbf{u}_1^t, \mathbf{u}_2^t, \dots, \mathbf{u}_N^t] \end{aligned} \quad (14)$$

First, the *rand* function samples uniformly from the range $[0, 1]$ to obtain a vector \mathbf{r}_i^t . Then get \mathbf{cr}_i^t from \mathbf{cr}^t according to the index. The *tile* function expands \mathbf{cr}_i^t into a d -dimensional vector: $[\mathbf{cr}_i^t, \mathbf{cr}_i^t, \dots, \mathbf{cr}_i^t]$. The *cat* function concatenates them into a matrix as shown below:

$$\begin{bmatrix} r_{i,1}^t & r_{i,2}^t & \cdots & r_{i,d}^t \\ \mathbf{cr}_i^t & \mathbf{cr}_i^t & \cdots & \mathbf{cr}_i^t \end{bmatrix} \quad (15)$$

Here, *gumbel_softmax* is executed column-wise. For any column, the larger element becomes 1 after *gumbel_softmax* and 0 otherwise. Therefore, $\mathbf{cv}_i^t \in \mathbb{R}^{2 \times d}$ may be a matrix like this:

$$\mathbf{cv}_i^t = \begin{bmatrix} 1 & 0 & 0 & 0 & 1 & 1 & \cdots & 1 & 1 \\ 0 & 1 & 1 & 1 & 0 & 0 & \cdots & 0 & 0 \end{bmatrix} \quad (16)$$

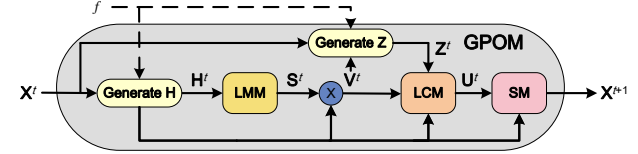


Figure 1. The overall architecture of GPOM.

Overall Framework The overall architecture of GPOM is shown in Fig. 1. The parameters that need to be trained in *GPOM* are $\theta = \{\theta_1, \theta_2\}$. At time step t , the population is \mathbf{X}^t . Initially, we amalgamate the information from \mathbf{X}^t to construct descriptive representations of the population, \mathbf{H}^t and \mathbf{Z}^t . *LMM* adaptively generates \mathbf{S}^t based on \mathbf{H}^t . The multiplication of \mathbf{X}^t and \mathbf{S}^t yields \mathbf{V}^t (see Eq. (4)). Next, *LCM* adaptively generates \mathbf{cr}^t based on its input \mathbf{Z}^t , and performs a crossover operation based on \mathbf{cr}^t to obtain \mathbf{U}^t . Finally, *SM* (Wu et al., 2023), a *1-to-1* selection strategy is executed between \mathbf{U}^t and \mathbf{X}^t to produce the next-generation population \mathbf{X}^{t+1} .

$$\begin{aligned} \mathbf{X}^{t+1} &= \text{SM}(\mathbf{X}^t, \mathbf{U}^t) \\ &= \text{tile}(l_{x>0}(\mathbf{M}_{F'} - \mathbf{M}_F)) \odot \mathbf{X}^t \\ &\quad + \text{tile}(1 - l_{x>0}(\mathbf{M}_{F'} - \mathbf{M}_F)) \odot \mathbf{U}^t \end{aligned} \quad (17)$$

where $l_{x>0}(x) = 1$ if $x > 0$ and $l_{x>0}(x) = 0$ if $x < 0$, and the *tile* copy function extends the indication matrix to a tensor with size (N, d) , $\mathbf{M}_F(\mathbf{M}_{F'})$ denotes the fitness matrix of $\mathbf{X}^t(\mathbf{U}^t)$, and \odot indicates the pairwise multiplication between inputs.

3.4. Tasks, Loss Function & MetaGBT

GPOM is meticulously crafted as a model amenable to end-to-end training based on gradients. While GPOM necessitates gradient information from the training task during the training phase, it exhibits the ability to tackle BBO problems

Algorithm 1 MetaGBT

Input: T, n , training set TS .
Output: The optimal θ .

- 1: Randomly sample the parameter θ of *GPOM*.
- 2: **while** not done **do**
- 3: Sample $|TS|$ populations of size n to obtain the population set $pop \leftarrow [\mathbf{X}_1^0, \mathbf{X}_2^0, \dots, \mathbf{X}_{|TS|}^0]$.
- 4: **for** $i = 1, 2, \dots, |TS|$ **do**
- 5: Randomly sample ω^i for the f_i in TS .
- 6: **end for**
- 7: **for** $t = 1, 2, \dots, T$ **do**
- 8: **for** $i = 1, 2, \dots, |TS|$ **do**
- 9: $\mathbf{X}_i^t \leftarrow GPOM(\mathbf{X}_i^{t-1}, 1|\theta)$.
- 10: $loss_i^t \leftarrow l_i(\mathbf{X}_i^t, \mathbf{X}_i^{t-1}, f_i, \omega^i)$.
- 11: **end for**
- 12: $\theta \leftarrow$ Update θ using gradient backpropagation algorithm based on $\frac{1}{|TS|} \sum_i loss_i^t$.
- 13: **end for**
- 14: **end while**

in the testing phase without relying on any gradient information. To ensure the acquisition of an efficient, highly robust, and broadly generalizable optimization strategy, GPOM undergoes training on a diverse set of tasks. Training on these tasks sequentially poses the risk of domain overfitting, local optima entrapment, and diminished generalization performance. Consequently, we introduce a training methodology named *MetaGBT*.

Table 1. Training functions. $z_i = x_i - \omega_i$.

ID	Functions	Range
TF1	$\sum_i x_i - \omega_i $	$x \in [-10, 10], \omega \in [-10, 10]$
TF2	$\sum_i (x_i - \omega_i) + (x_{i+1} - \omega_{i+1}) + \sum_i x_i - \omega_i $	$x \in [-10, 10], \omega \in [-10, 10]$
TF3	$\sum_i z_i^2$	$x \in [-100, 100], \omega \in [-50, 50]$
TF4	$\max\{ z_i , 1 \leq i \leq d\}$	$x \in [-100, 100], \omega \in [-50, 50]$

Tasks We form a training task set $TS = \{f_i(\mathbf{X}|\omega^j)\}$, where $i \in [1, 4]$ and $j \in [1, N]$, comprising $4N$ tasks derived from Table 1, where ω_i denotes the task parameter influencing the function’s landscape offset. Our selection of these functions for the training task is motivated by their diverse landscape features. The specific landscape features encompassed in TS are detailed in Appendix B.

Loss Function To avoid bias of different output scales in TS , for any function f_i in TS , we design the normalized loss function $l_i(\mathbf{X}^t, \mathbf{X}^{t-1}, f_i, \omega^i)$. Equation (18) calculates the average fitness difference between the input and output

of GPOM, further normalized within $[0, 1]$.

$$\mathbf{X}^t = GPOM(\mathbf{X}^{t-1}, 1|\theta)$$

$$l_i = \frac{\frac{1}{|\mathbf{X}^t|} \sum_{\mathbf{x} \in \mathbf{X}^t} f_i(\mathbf{x}|\omega^i) - \frac{1}{|\mathbf{X}^{t-1}|} \sum_{\mathbf{x} \in \mathbf{X}^{t-1}} f_i(\mathbf{x}|\omega^i)}{\left| \frac{1}{|\mathbf{X}^{t-1}|} \sum_{\mathbf{x} \in \mathbf{X}^{t-1}} f_i(\mathbf{x}|\omega^i) \right|} \quad (18)$$

MetaGBT The pseudocode for *MetaGBT* is presented in Algorithm 1. Initially, we sample the *GPOM* parameter θ from a standard normal distribution. The objective of *MetaGBT* is to iteratively update θ to bring it closer to the global optimum θ^* . In line 2, we sample a population for each task in TS . Lines 3, 4 and 5 involve the resampling of task parameters for all tasks in TS , thereby altering the task landscape, augmenting training complexity, and enhancing the learning of robust optimization strategies by GPOM. The final loss function (line 10) is determined by computing the average of the loss functions for all tasks. Subsequently, in line 12, we update θ using a gradient-based optimizer, such as Adam (Kingma & Ba, 2014). The trained *GPOM* is then ready for application in solving an unknown BBO problem, as depicted in Algorithm 2.

Algorithm 2 Driving GPOM to Solve Problem

Input: Generations T , population size n , BBO problem f .
Output: The optimal \mathbf{X}^T found.

- 1: *GPOM* loads the trained parameter θ .
- 2: Randomly sample an initial population \mathbf{X}^0 of size n .
- 3: **for** $t = 0, 1, \dots, T - 1$ **do**
- 4: Construct \mathbf{H}^t based on \mathbf{X}^t and f .
- 5: $\mathbf{S}^t \leftarrow LMM(\mathbf{H}^t|\theta_1)$.
- 6: $\mathbf{V}^t \leftarrow \mathbf{S}^t \times \mathbf{X}^t$.
- 7: Build \mathbf{Z}^t based on \mathbf{X}^t , \mathbf{V}^t and f .
- 8: $\mathbf{cr}^t \leftarrow LCM(\mathbf{Z}^t|\theta_2)$.
- 9: Construct \mathbf{U}^t using Equation (14).
- 10: $\mathbf{X}^{t+1} \leftarrow SM(\mathbf{X}^t, \mathbf{U}^t)$.
- 11: **end for**

4. Experiments

4.1. Experimental Setup

We test the performance of GPOM on the widely used BBO benchmark and two complex real-world problems (see Appendix C). Selected methods include DE (DE/rand/1/bin) (Das & Suganthan, 2010) and ES ((μ, λ)-ES) as population-based baselines, L-SHADE (Tanabe & Fukunaga, 2014) and CMA-ES (Hansen, 2016) as state-of-the-art population-based BBO methods, and LES (Lange et al., 2023b) and LGA (Lange et al., 2023a) as state-of-the-art POMs. GPOM is trained on TS with $T = 100$, $n = 100$, and $d = 10$. Detailed parameters for all compared methods are provided

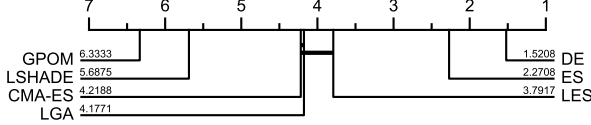


Figure 2. The critical difference diagram illustrates the performance ranking of seven algorithms across 24 BBOB problems with dimensions $d = 30, 100$, employing Wilcoxon-Holm analysis (Ismail Fawaz et al., 2019) at a significance level of $p = 0.05$. Algorithm positions are indicative of their mean scores across multiple datasets, with higher scores signifying a method consistently outperforming competitors. Thick horizontal lines denote scenarios where there is no statistically significant difference in algorithm performance.

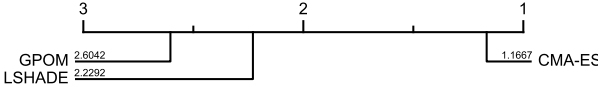


Figure 3. Critical difference diagram of 3 algorithms on 24 BBOB problems with $d = 100$. The locations of the optimal solutions are in the range of $[-1, 1]$.

in Appendix E. Please refer to Appendix D for the reasons for choosing these algorithms.

4.2. Results

BBOB (Hansen et al., 2021) We evaluate the generalization ability of GPOM across 24 BBOB functions with dimensions $d = 30$ and $d = 100$, where optimal solutions are located at **0**. Figure 2 presents the critical difference diagram comparing all algorithms (refer to Appendix Tables 5 and 7, and Figures 11, 12 and 13 for detailed results). GPOM significantly outperforms all methods, showcasing its efficacy across varying dimensions. Despite being trained solely on TF1-TF4 with $d = 10$, GPOM excels in higher dimensions ($d = \{30, 100, 500\}$), with its performance advantage becoming more pronounced with increasing dimensionality. Particularly on complex problems F21-F24, where global structure is weak, GPOM lags behind LSHADE but surpasses other methods, attributed to its adaptability through fine-tuning. Additional experimental results in Figure 3 (see Appendix F.2 for details) demonstrate GPOM’s superior performance even when optimal solutions are perturbed within the range of $[-1, 1]$.

We provide further experimental results in Figure 3 (see Appendix F.2 for more information), where the optimal solutions of the functions have been disturbed in the range of $[-1, 1]$. The performance of GPOM still dominates that of other algorithms, as shown in Figure 3.

Bipedal Walker (Brockman et al., 2016) The Bipedal Walker task involves optimizing a fully connected neural

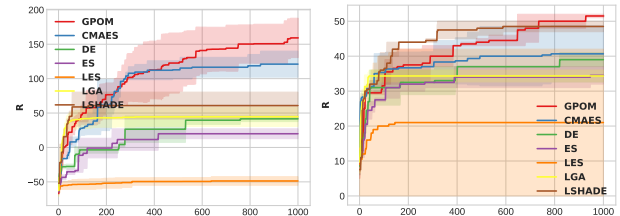


Figure 4. Experimental results are presented for the Bipedal Walker (a) and Enduro (b), with the vertical axis denoted as R , representing the strategy score. The score corresponds to the total reward acquired by the agent during interactions with the environment.

network with $d = 874$ parameters over $k = 800$ time steps to enhance robot locomotion control. In Fig. 4(a), LSHADE shows ineffectiveness, while CMA-ES, LSHADE, and LGA suffer from premature convergence. Conversely, GPOM achieves stable and swift convergence, ultimately attaining the highest score.

Enduro (Brockman et al., 2016) Enduro task entails controlling a strategy with $d = 4149$ parameters across $k = 500$ steps, posing greater difficulty than Bipedal Walker. As depicted in Fig. 4(b), LGA and LES exhibit premature convergence and limited exploration. While CMA-ES initially converges slightly faster than GPOM, the latter maintains a superior balance between exploration and exploitation, outperforming LSHADE.

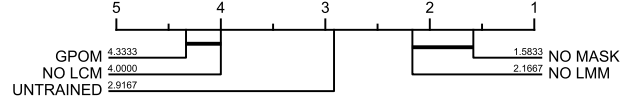


Figure 5. Results of ablation study. The metric used to evaluate performance is the optimal value of the function found, with smaller values being better. Here, $d = 30$.

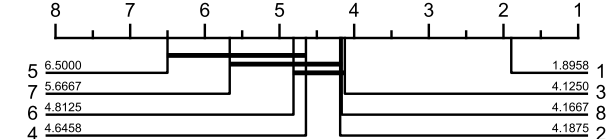


Figure 6. The impact of training dataset size on the performance of GPOM. $d = 100$.

4.3. Analysis

Ablation Study The ablation study results for the designed modules are presented in Fig. 5 (refer to Appendix Table 8 for additional details). Configurations include *UNTRAINED*, representing an untrained GPOM with randomly initialized parameters; *NO LMM*, where the LMM is excluded, and a simple *DE/rand/1/bin* mutation operator is

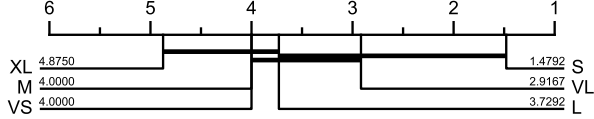


Figure 7. Results of GPOMs with different sizes on BBOB tests ($d = 100$).

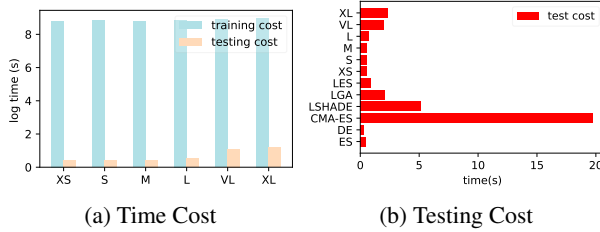


Figure 8. The Time Cost of GPOM

employed; *NO LCM*, indicating the absence of the learnable crossover operation, using only binomial crossover; and *NO MASK*, signifying the omission of the mask operation described in Eq. (11).

While *UNTRAINED* yields optimal results for F9 and F16, as an untrained GPOM is inherently an optimization strategy, the adaptability of trained GPOM surpasses the baselines in most scenarios. In simpler tasks with $d = 30$, *UNTRAINED* underperforms, demonstrating the advantage of trained GPOM on more complex tasks. Notably, *NO LMM* and *NO LCM* excel on F5, F11, and F19, respectively. This could be attributed to potential overfitting of GPOM to the relatively simple training set. The exclusion of mask operation (*NO MASK*) significantly diminishes GPOM’s performance, highlighting the importance of the mask for global information sharing and population interaction, crucial for maintaining diversity. All modules contribute to GPOM’s overall performance, with the negative impact on GPOM’s performance ranked as follows: *NO MASK* > *NO LMM* > *UNTRAINED* > *NO LCM*.

Training Dataset We further investigate the influence of training data scale on GPOM, employing four additional functions detailed in Appendix Table 4 for experimental analysis, with corresponding results displayed in Fig. 6 (refer to Appendix Table 9 for additional details). Numeric labels, from 1 to 8, signify the inclusion of TF1 to TF8 during GPOM training. The choice of the training set significantly impacts GPOM’s performance. Noteworthy observations emerge: 1) Utilizing TF1-TF4 leads to enhanced algorithm performance as the number of functions increases; 2) Introduction of TF5, TF6, and TF7 provides marginal performance improvement; 3) Incorporating TF8 results in a notable performance decline, suggesting that increased function diversity does not necessarily boost GPOM performance. The complexity of TF8 might induce overfitting,

diminishing GPOM’s generalization capability. This underscores the importance of balancing simplicity and complexity when constructing the training set, as overly complex functions can adversely affect performance.

Scale of GPOM We explore the performance of GPOM at different scales, which is shown in Fig. 7 (refer to Appendix Table 10 for additional details). We increase GPOM’s parameter count by perturbing the hidden layers of each module (d_m, d_c). Six models are constructed in ascending order of parameter count, labeled as *VS* (very small), *S* (small), *M* (medium), *L* (large), *VL* (very large), and *XL* (extra large) (details in the Appendix Table 3). *XL* achieves the best performance, while *VS* and *M* also perform well. *S* exhibits the worst performance, and *VL* performs worse than *L*. Two core factors contribute to this phenomenon: the number of parameters and training difficulty. *VS*, with the fewest parameters, is the easiest to train and performs well on BBOB. Conversely, *XL*, with a large number of parameters, exhibits the strongest capability to represent strategies, resulting in the best performance. The performance of *XL* aligns with our expectations. We obtain the following principles: 1) Larger models can have stronger capabilities but are more challenging to train; 2) Training difficulty and model scale do not exhibit a simple linear relationship, warranting further research; 3) Larger models require more functions for effective training.

Time Budget We assess the training and test time efficiency of GPOM across various architectures on BBOB ($d = 10$) and BBOB ($d = 100$) respectively, as illustrated in Figure 8. GPOM demonstrates remarkable efficiency in tackling BBO problems, with negligible training costs relative to its exceptional generalization ability and high performance.

4.4. Visualization Analysis

LMM Learning Analysis Figure 9 displays S^t for an in-depth analysis of the LMM strategy (refer to Appendix Figure 14-19 for additional details). Key observations and conclusions include: 1) Generally, superior individuals receive higher weights during LMM, showcasing GPOM’s ability to balance exploration and exploitation as the population converges. 2) Across diverse function problems, GPOM dynamically generates optimization strategies, highlighting its adaptability and contributing to robust generalization. 3) Disadvantaged individuals exhibit a more uniform weight distribution, potentially aiding in their escape from local optima and enhancing algorithm convergence.

LCM Learning Analysis We visually examine the LCM strategy, presenting the results in Fig. 10 (refer to Appendix

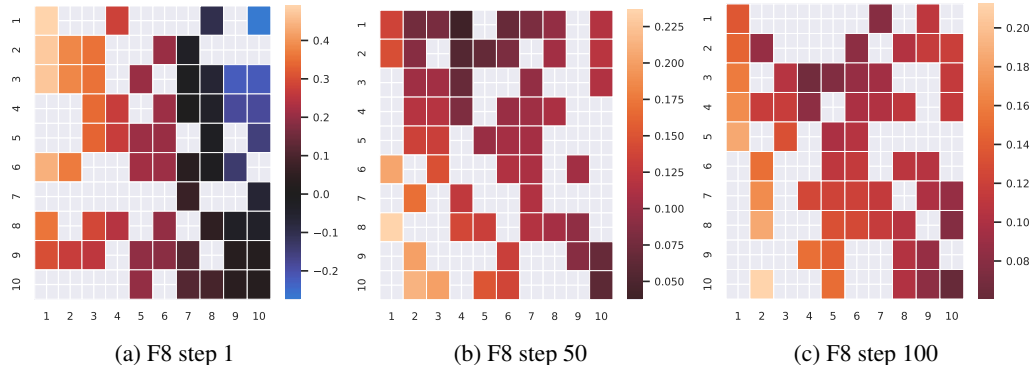


Figure 9. Displayed are visualized outcomes of LMM S^t in BBOB with $d = 100$ using $n = 10$ for clarity. Blank squares in the matrix denote masked portions from Eq. (11). Steps 1, 50, and 100 correspond to the 1st, 50th, and 100th generations in population evolution. The horizontal and vertical axes denote individual rankings, with 1 as the best and 10 as the worst in the population. Each row illustrates the weight assigned to other individuals when executing mutation operations for the respective individual.

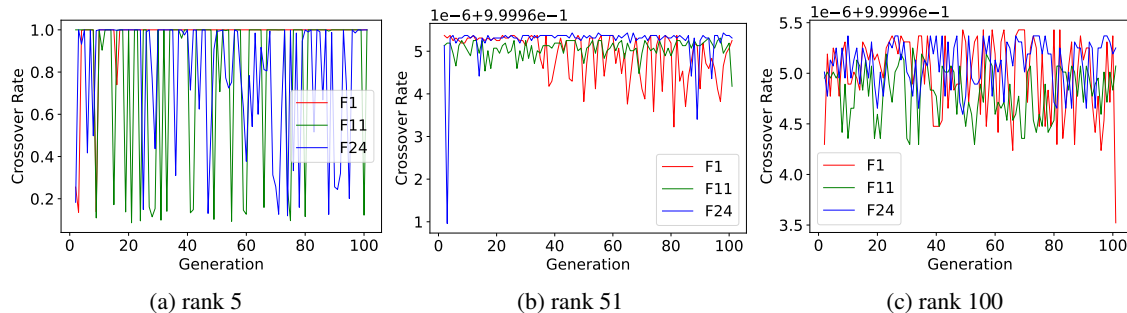


Figure 10. Visual analysis results of LCM on BBOB F1, F11, and F24 with $d = 100$, employing $n = 100$, are presented. "Rank" signifies an individual's position, with rank 5 representing the fifth-ranked individual in the population. Subgraphs depict the evolution of the probability that an individual will undergo crossover across three tasks as the population progresses. For example, (a) illustrates the crossover probability change for the top-ranked individual on F1, F11, and F24 with the number of generations.

Figure 20-25 for additional details). LCM displays the capacity to adaptively generate diverse strategies for individuals across different ranks in the population, revealing distinct patterns among tasks and rankings. Notably, top-ranking individuals within the top 20, such as those ranked 1st, 5th, and 18th, exhibit a flexible crossover strategy. The dynamic adjustment of crossover probability with population evolution aids in preserving dominant genes and facilitating escape from local optima. Conversely, lower-ranking individuals show an increasing overall probability of crossover, promoting exploration of disadvantaged individuals and enhancing the algorithm's exploration capability. LCM proficiently generates adaptive crossover strategies across tasks, individuals, and convergence stages, significantly boosting both convergence and exploration capabilities.

5. Conclusions

We present GPOM, a novel General Pretrained Optimization Model, addressing inefficiencies in existing methods. GPOM, a population-based pretrained BBO model, lever-

ages Differential Evolution (DE) mechanisms with mutation, crossover, and selection operators. Modules like LMM and LCM equip GPOM with advanced optimization capabilities. Pretraining GPOM ensures robust convergence and generalization. Evaluation on BBOB and robot control tasks demonstrates GPOM’s superiority over other pretrained optimization models, even in high-dimensional scenarios. GPOM’s adaptive optimization strategy and remarkable generalization mark significant advancements, addressing key challenges in existing models.

Further research avenues include: 1) Designing enhanced loss functions to optimize GPOM for both population convergence and diversity, thus enhancing algorithm performance. 2) The correlation between the training set and test problem may impact GPOM's performance during testing. To mitigate this, employing a "pre-training + fine-tuning" approach could be beneficial. This involves pre-training GPOM on various tasks followed by fine-tuning on the specific target problem with few samples to improve its efficacy in solving the target task.

6. Potential Impact

This paper presents work whose goal is to advance the field of Machine Learning. There are many potential societal consequences of our work, none which we feel must be specifically highlighted here.

References

- Bali, K. K., Ong, Y.-S., Gupta, A., and Tan, P. S. Multifactorial evolutionary algorithm with online transfer parameter estimation: Mfea-ii. *IEEE Transactions on Evolutionary Computation*, 24(1):69–83, 2019.
- Brockman, G., Cheung, V., Pettersson, L., Schneider, J., Schulman, J., Tang, J., and Zaremba, W. Openai gym, 2016.
- Chen, A., Dohan, D. M., and So, D. R. Evoprompting: Language models for code-level neural architecture search. *arXiv preprint arXiv:2302.14838*, 2023.
- Chen, S., Montgomery, J., and Bolufé-Röhler, A. Measuring the curse of dimensionality and its effects on particle swarm optimization and differential evolution. *Applied Intelligence*, 42:514–526, 2015.
- Chen, Y., Song, X., Lee, C., Wang, Z., Zhang, R., Dohan, D., Kawakami, K., Kochanski, G., Doucet, A., Ranzato, M., et al. Towards learning universal hyperparameter optimizers with transformers. *Advances in Neural Information Processing Systems*, 35:32053–32068, 2022.
- Das, S. and Suganthan, P. N. Differential evolution: A survey of the state-of-the-art. *IEEE transactions on evolutionary computation*, 15(1):4–31, 2010.
- Das, S., Mullick, S. S., and Suganthan, P. N. Recent advances in differential evolution—an updated survey. *Swarm and evolutionary computation*, 27:1–30, 2016.
- Deb, K., Pratap, A., Agarwal, S., and Meyarivan, T. A fast and elitist multiobjective genetic algorithm: Nsga-ii. *IEEE Transactions on Evolutionary Computation*, 6(2):182–197, 2002.
- Finck, S., Hansen, N., Ros, R., and Auger, A. Real-parameter black-box optimization benchmarking 2009: Presentation of the noiseless functions. Technical report, Citeseer, 2010.
- Finn, C., Abbeel, P., and Levine, S. Model-agnostic meta-learning for fast adaptation of deep networks. In *International conference on machine learning*, pp. 1126–1135. PMLR, 2017.
- Gämperle, R., Müller, S. D., and Koumoutsakos, P. A parameter study for differential evolution. *Advances in intelligent systems, fuzzy systems, evolutionary computation*, 10(10):293–298, 2002.
- Gomes, H. S., Léger, B., and Gagné, C. Meta learning black-box population-based optimizers. *arXiv preprint arXiv:2103.03526*, 2021.
- Gong, Y.-J., Li, J.-J., Zhou, Y., Li, Y., Chung, H. S.-H., Shi, Y.-H., and Zhang, J. Genetic learning particle swarm optimization. *IEEE Transactions on Cybernetics*, 46(10):2277–2290, 2015.
- Hansen, N. The cma evolution strategy: A tutorial. *arXiv preprint arXiv:1604.00772*, 2016.
- Hansen, N. and Ostermeier, A. Completely derandomized self-adaptation in evolution strategies. *Evolutionary Computation*, 9(2):159–195, 2001.
- Hansen, N., Müller, S. D., and Koumoutsakos, P. Reducing the time complexity of the derandomized evolution strategy with covariance matrix adaptation (cma-es). *Evolutionary computation*, 11(1):1–18, 2003.
- Hansen, N., Auger, A., Ros, R., Mersmann, O., Tušar, T., and Brockhoff, D. Coco: A platform for comparing continuous optimizers in a black-box setting. *Optimization Methods and Software*, 36(1):114–144, 2021.
- Holland, J. H. Genetic algorithms. *Scientific american*, 267(1):66–73, 1992.
- Hutter, F., Kotthoff, L., and Vanschoren, J. *Automated machine learning: methods, systems, challenges*. Springer Nature, 2019.
- Ismail Fawaz, H., Forestier, G., Weber, J., Idoumghar, L., and Muller, P.-A. Deep learning for time series classification: a review. *Data Mining and Knowledge Discovery*, 33(4):917–963, 2019.
- Jang, E., Gu, S., and Poole, B. Categorical reparameterization with gumbel-softmax. *arXiv preprint arXiv:1611.01144*, 2016.
- Jazzbin. Geatpy: The genetic and evolutionary algorithm toolbox with high performance in python, 2020.
- Kennedy, J. and Eberhart, R. Particle swarm optimization. In *Proceedings of ICNN'95-International Conference on Neural Networks*, volume 4, pp. 1942–1948. IEEE, 1995.
- Kingma, D. P. and Ba, J. Adam: A method for stochastic optimization. *arXiv preprint arXiv:1412.6980*, 2014.
- Krishnamoorthy, S., Mashkaria, S. M., and Grover, A. Generative pretraining for black-box optimization. *arXiv preprint arXiv:2206.10786*, 2022.

- Krishnamoorthy, S., Mashkaria, S. M., and Grover, A. Diffusion models for black-box optimization. *arXiv preprint arXiv:2306.07180*, 2023.
- Lange, R., Schaul, T., Chen, Y., Lu, C., Zahavy, T., Dalibard, V., and Flennberg, S. Discovering attention-based genetic algorithms via meta-black-box optimization. In *Proceedings of the Genetic and Evolutionary Computation Conference*, pp. 929–937, 2023a.
- Lange, R., Schaul, T., Chen, Y., Zahavy, T., Dalibard, V., Lu, C., Singh, S., and Flennberg, S. Discovering evolution strategies via meta-black-box optimization. In *Proceedings of the Companion Conference on Genetic and Evolutionary Computation*, pp. 29–30, 2023b.
- Lehman, J., Gordon, J., Jain, S., Ndousse, K., Yeh, C., and Stanley, K. O. Evolution through large models. In *Handbook of Evolutionary Machine Learning*, pp. 331–366. Springer, 2023.
- Liu, F., Tong, X., Yuan, M., and Zhang, Q. Algorithm evolution using large language model. *arXiv preprint arXiv:2311.15249*, 2023a.
- Liu, R., Gao, J., Zhang, J., Meng, D., and Lin, Z. Investigating bi-level optimization for learning and vision from a unified perspective: A survey and beyond. *IEEE Transactions on Pattern Analysis and Machine Intelligence*, 44(12):10045–10067, 2022. doi: 10.1109/TPAMI.2021.3132674.
- Liu, S., Chen, C., Qu, X., Tang, K., and Ong, Y.-S. Large language models as evolutionary optimizers. *arXiv preprint arXiv:2310.19046*, 2023b.
- Ma, Y. J., Liang, W., Wang, G., Huang, D.-A., Bastani, O., Jayaraman, D., Zhu, Y., Fan, L., and Anandkumar, A. Eureka: Human-level reward design via coding large language models. *arXiv preprint arXiv:2310.12931*, 2023.
- Meyerson, E., Nelson, M. J., Bradley, H., Moradi, A., Hoover, A. K., and Lehman, J. Language model crossover: Variation through few-shot prompting. *arXiv preprint arXiv:2302.12170*, 2023.
- Nasir, M. U., Earle, S., Togelius, J., James, S., and Cleghorn, C. Llmatric: Neural architecture search via large language models and quality-diversity optimization. *arXiv preprint arXiv:2306.01102*, 2023.
- Neri, F. and Tirronen, V. Recent advances in differential evolution: a survey and experimental analysis. *Artificial intelligence review*, 33:61–106, 2010.
- Romera-Paredes, B., Barekatain, M., Novikov, A., Balog, M., Kumar, M. P., Dupont, E., Ruiz, F. J., Ellenberg, J. S., Wang, P., Fawzi, O., et al. Mathematical discoveries from program search with large language models. *Nature*, pp. 1–3, 2023.
- Ronkkonen, J., Kukkonen, S., and Price, K. V. Real-parameter optimization with differential evolution. In *2005 IEEE congress on evolutionary computation*, volume 1, pp. 506–513. IEEE, 2005.
- Ros, R. and Hansen, N. A simple modification in cma-es achieving linear time and space complexity. In *International Conference on Parallel Problem Solving from Nature*, pp. 296–305. Springer, 2008.
- Shala, G., Biedenkapp, A., Awad, N., Adriaensen, S., Lindauer, M., and Hutter, F. Learning step-size adaptation in cma-es. In *International Conference on Parallel Problem Solving from Nature*, pp. 691–706. Springer, 2020.
- Stanovov, V., Akhmedova, S., and Semenkin, E. Nl-shade-lbc algorithm with linear parameter adaptation bias change for cec 2022 numerical optimization. In *2022 IEEE Congress on Evolutionary Computation (CEC)*, pp. 01–08. IEEE, 2022.
- Storn, R. and Price, K. Differential evolution—a simple and efficient heuristic for global optimization over continuous spaces. *Journal of global optimization*, 11:341–359, 1997.
- Such, F. P., Madhavan, V., Conti, E., Lehman, J., Stanley, K. O., and Clune, J. Deep neuroevolution: Genetic algorithms are a competitive alternative for training deep neural networks for reinforcement learning. *arXiv preprint arXiv:1712.06567*, 2017.
- Tanabe, R. and Fukunaga, A. S. Improving the search performance of shade using linear population size reduction. In *2014 IEEE Congress on Evolutionary Computation (CEC)*, pp. 1658–1665, 2014. doi: 10.1109/CEC.2014.6900380.
- Thangaraj, R., Pant, M., and Abraham, A. A simple adaptive differential evolution algorithm. In *2009 world congress on nature & biologically inspired computing (nabic)*, pp. 457–462. IEEE, 2009.
- Tvrdík, J. Competitive differential evolution. In *Mendel*, pp. 7–12, 2006.
- Vaswani, A., Shazeer, N., Parmar, N., Uszkoreit, J., Jones, L., Gomez, A. N., Kaiser, Ł., and Polosukhin, I. Attention is all you need. *Advances in neural information processing systems*, 30, 2017.
- Wolpert, D. H. and Macready, W. G. No free lunch theorems for optimization. *IEEE transactions on evolutionary computation*, 1(1):67–82, 1997.

Wu, K., Liu, P., and Liu, J. Deen: Automated evolutionary algorithms via evolution inspired deep convolution network, 2023.

Xu, J., Sun, X., Zhang, Z., Zhao, G., and Lin, J. Understanding and improving layer normalization. *Advances in Neural Information Processing Systems*, 32, 2019.

Yang, C., Wang, X., Lu, Y., Liu, H., Le, Q. V., Zhou, D., and Chen, X. Large language models as optimizers. *arXiv preprint arXiv:2309.03409*, 2023.

Ye, Q., Sun, Y., Zhang, J., and Lv, J. A distributed framework for ea-based nas. *IEEE Transactions on Parallel and Distributed Systems*, 32(7):1753–1764, 2021. doi: 10.1109/TPDS.2020.3046774.

Yu, Y., Lei, Z., Wang, Y., Zhang, T., Peng, C., and Gao, S. Improving dendritic neuron model with dynamic scale-free network-based differential evolution. *IEEE/CAA Journal of automatica sinica*, 9(1):99–110, 2021.

Zhang, X., Clune, J., and Stanley, K. O. On the relationship between the openai evolution strategy and stochastic gradient descent. *arXiv preprint arXiv:1712.06564*, 2017.

A. Mutation Strategy in DE

We list some classic DE mutation strategies.

- DE/rand/1

$$\mathbf{v}_i^t = \mathbf{x}_{r1}^t + F \cdot (\mathbf{x}_{r2}^t - \mathbf{x}_{r3}^t) \quad (19)$$

- DE/rand/2

$$\mathbf{v}_i^t = \mathbf{x}_{r1}^t + F \cdot (\mathbf{x}_{r2}^t - \mathbf{x}_{r3}^t + \mathbf{x}_{r4}^t - \mathbf{x}_{r5}^t) \quad (20)$$

- DE/best/1

$$\mathbf{v}_i^t = \mathbf{x}_{best}^t + F \cdot (\mathbf{x}_{r1}^t - \mathbf{x}_{r2}^t) \quad (21)$$

- DE/current-to-rand/1

$$\mathbf{v}_i^t = (1 - F)\mathbf{x}_i^t + F \cdot (\mathbf{x}_{r1}^t - \mathbf{x}_{r2}^t + \mathbf{x}_{r3}^t) \quad (22)$$

- DE/current-to-best/1

$$\mathbf{v}_i^t = (1 - F)\mathbf{x}_i^t + F \cdot \mathbf{x}_{best}^t + F \cdot (\mathbf{x}_{r1}^t - \mathbf{x}_{r2}^t) \quad (23)$$

- DE/current-to-pbest/1

$$\mathbf{v}_i^t = (1 - F)\mathbf{x}_i^t + F \cdot \mathbf{x}_{pbest}^t + F \cdot (\mathbf{x}_{r1}^t - \mathbf{x}_{r2}^t) \quad (24)$$

The integer index $r1$ (and similarly, $r2$ and $r3$) is randomly selected from the range $[0, N]$. $pbest$ is randomly selected from the indices of the best p individuals. x_{best}^t is the individual with the best fitness in the population at generation t .

The generalized form of the mutation strategy is

$$\mathbf{v}_i^t = \sum_j^N w_{i,j} \mathbf{x}_j \quad (\forall w_{i,j} \in \mathbb{R}) \quad (25)$$

For example, when $w_{i,q} = 1, w_{i,k} = -w_{i,j} \neq 0$, and $w_{i,l} = 0$ ($\forall l \notin \{q, j, k\}, q \neq k, k \neq j, q \neq j$), it becomes DE/rand1/1. If individuals of the population has been sorted from good to bad by fitness, when $w_{i,0} = 1, w_{i,k} = -w_{i,j} \neq 0$, and $w_{i,l} = 0$ ($\forall l \notin \{0, j, k\}, k \neq j$), it becomes DE/best/1.

B. Landscape Features of TF1-Tf8

The landscape features included in TS are shown as follows:

- TF1: Unimodal
- TF2: Separable
- TF3: Unimodal, Separable
- TF4: Unimodal, Separable
- TF5: Multimodal, Non-separable, Having a very narrow valley from local optimum to global optimum, Ill-conditioned
- TF6: Multimodal, Separable, Asymmetrical, Local optima's number is huge
- TF7: Multi-modal, Non-separable, Rotated
- TF8: Multi-modal, Non-separable, Asymmetrical

C. Test Set

C.1. BBOB

BBOB (Finck et al., 2010; Hansen et al., 2021) is a widely researched and recognized collection of benchmark test problems to evaluate the performance of optimization algorithms. The dataset consists of a series of high-dimensional continuous optimization functions, including single-peak, multi-peak, rotated, and distorted functions, as well as some functions with specific properties such as Lipschitz continuity and second-order differentiability.

C.2. Robot Control Tasks

We test the performance of GPOM on two complex robot control tasks.

C.2.1. BIPEDAL WALKER

The continuous control task Bipedal Walker (Brockman et al., 2016), implemented within the Box2D physics engine, has been designed to test the ability of walking agents to navigate varying terrain by controlling their joints and maintaining balance. The challenge requires the agent to learn efficient walking strategies that enable it to traverse the intended path without falling or deviating from its trajectory. The robot's state comprises a range of variables, including the hull angle speed, angular velocity, horizontal speed, vertical speed, joint positions and angular speeds, legs contact with the ground, and lidar rangefinder measurements. The robot's actions involve determining motor speed values in the range of [-1, 1] for each of the four joints at the hips and knees. The performance of the agent is evaluated through a reward system, whereby it receives points for moving forward, with a maximum of 300+ points awarded upon successfully reaching the end of the designated course. However, the penalty of -100 points is imposed if the robot loses balance and falls. Furthermore, applying motor torque incurs a small cost in terms of points. The score accrued by the agent serves as a measure of its optimal performance. The Bipedal Walker task represents a challenging and dynamic environment that effectively evaluates the walking and balance control abilities of agents. As such, it provides a valuable benchmark for testing and comparing different reinforcement learning algorithms for robotic locomotion.

C.2.2. ENDURO

Enduro (Brockman et al., 2016) is one of the classic reinforcement learning environments provided by OpenAI Gym. It is a driving racing game based on the Atari 2600 game. In this environment, your goal is to drive as far as possible by controlling the car. The Enduro game is set on an endless highway where you need to avoid other vehicles and overtake as many other vehicles as possible within a limited time. You can avoid collisions with other vehicles by moving your car left and right, and be careful to control your speed to avoid accidents. The game rewards you based on how far you drive, so your goal is to learn a good driving strategy to maximize the distance traveled.

In these two test tasks, the agent interacts with the environment for k time steps, and the reward at the i -th step is r_i . We evaluate strategy performance as follows:

$$R = \sum_{i=0}^k r_i \quad (26)$$

D. Baselines

Our core is the population-based pre-training BBO algorithm, so we do not compare with non-population methods such as Bayesian optimization methods. Moreover, Bayesian optimization methods are difficult to deal with continuous optimization problems of more than 100 dimensions. We do not use LLM-based approaches (Romera-Paredes et al., 2023; Meyerson et al., 2023; Liu et al., 2023a; Yang et al., 2023; Lehman et al., 2023; Ma et al., 2023; Chen et al., 2023; Nasir et al., 2023) as baselines because they can only be used for a specific type of task.

Heuristic Population-based BBO Algorithm. DE(DE/rand/1/bin) (Das & Suganthan, 2010), ES((μ, λ) -ES), L-SHADE (Tanabe & Fukunaga, 2014), and CMA-ES (Hansen, 2016), where DE (Das & Suganthan, 2010) and ES are implemented based on Geatpy (Jazzbin, 2020), CMA-ES and IPOPCMA-ES are implemented by cmaes¹, and L-SHADE is implemented by pyade². The reasons for choosing these baselines are the following:

- DE(DE/rand/1/bin): A classic numerical optimization algorithm.
- ES((μ, λ) -ES): A classic variant of the evolution strategy.
- CMA-ES: CMA-ES is often considered the state-of-the-art method for continuous domain optimization under challenging settings (e.g., ill-conditioned, non-convex, non-continuous, multimodal).
- L-SHADE: The state-of-the-art variant of DE.

Pretrained BBO Algorithm. We chose three state-of-the-art meta-learn BBO algorithms for comparison with GPOM.

- LES (Lange et al., 2023b): A recently proposed learnable ES. It uses a data-driven approach to discover new ES with strong generalization performance and search efficiency.
- LGA (Lange et al., 2023a): A recently proposed learnable GA that discovers new GA in a data-driven manner. The learned algorithm can be applied to unseen optimization problems, search dimensions, and evaluation budgets.
- We train GPOM on *TS*. During training, the maximum number of evolution generations is 100, $n = 100$ and the problem dimension is set to 10.

¹<https://github.com/CyberAgentAILab>

²<https://github.com/xKuZz/pyade>

E. Parameters and Training Dataset

The primary control parameters of CMA-ES and L-SHADE are automatically adjusted. For LGA and LES, we utilized the optimal parameters provided by the authors without modifications. Other hyperparameters were tuned using grid search to identify the optimal combinations, and multiple experiments were conducted accordingly. Detailed parameter settings are presented in Table 2. Each experiment reports the mean and standard deviation of the results from various sets of experiments, with a consistent population size of 100 across all trials.

Table 2. Detailed parameter settings for all baselines.

Algorithm	item	setting
GPOM	$d_m = 1000$	Standard Settings for GPOM (M).
	$d_c = 4$	
CMA-ES	Initial $\sigma = \frac{\text{upper_bounds} + \text{lower_bounds}}{2} * \frac{2}{5}$	$2/5$ is a hyperparameter, and we determine this hyperparameter between $[0.1, 1]$ using a grid search, with a step of 0.1.
	Initial μ	$\mu = \text{lower_bounds} + (\text{randn}(d) * (\text{upper_bounds} - \text{lower_bounds}))$, where $\text{randn}(d)$ stands for sampling a d -dimensional vector from a standard normal distribution.
LSHADE	$\text{memory_size} = 6$	We use a grid search to determine this parameter, the search interval is $[1, 10]$, and the search step is 1.
ES	$\text{selFuc} = \text{urs}$	We use a grid search to determine this parameter, the search interval is $[\text{dup}, \text{ecs}, \text{etour}, \text{otos}, \text{rcs}, \text{rps}, \text{rws}, \text{sus}, \text{tour}, \text{urs}]$ (Jazzbin, 2020).
	$N_{\text{sel}} = 0.5$	we determine this hyperparameter between $[0.1, 0.8]$ using a grid search, with a step of 0.1.
DE	$F = 0.5$	we determine this hyperparameter between $[0.1, 0.9]$ using a grid search, with a step of 0.1. (Jazzbin, 2020).
	$XOVR = 0.5$	we determine this hyperparameter between $[0.1, 0.9]$ using a grid search, with a step of 0.1.
LGA LES	All parameters	We use the pre-trained optimal parameters provided by the authors.

Table 3. GPOM parameters of different architectures and architecture settings.

STRUCTURE	number of parameters	d_m	d_c
VS	1837	200	4
S	3637	500	4
M	6637	1000	4
L	12765	2000	20
VL	31005	5000	50
XL	61405	10000	100

Table 4. Additional Training Functions. $z_i = x_i - \omega_i$.

ID	Functions	Range
TF5(Rosenbrock)	$\sum_{i=1}^{d-1} (100(z_i^2 - z_{i+1})^2 + (z_i - 1)^2)$	$x \in [-100, 100], \omega \in [-50, 50]$
TF6(Rastrigin)	$\sum_{i=1}^d (z_i^2 - 10 \cos(2\pi z_i) + 10)$	$x \in [-5, 5], \omega \in [-2.5, 2.5]$
TF7(Griewank)	$\sum_{i=1}^d \frac{z_i^2}{4000} - \prod_{i=1}^d \cos(\frac{z_i}{\sqrt{i}}) + 1$	$x \in [-600, 600], \omega \in [-300, 300]$
TF8(Ackley)	$-20 \exp(-0.2 \sqrt{\frac{1}{d} \sum_{i=1}^d z_i^2}) - \exp(\frac{1}{d} \sum_{i=1}^d \cos(2\pi z_i)) + 20 + \exp(1)$	$x \in [-32, 32], \omega \in [-16, 16]$

F. Additional Experimental results on BBOB

F.1. BBOB Test

Table 5. BBOB RESULT. GPOM is trained on TF1-Tf4 with $d = 10$. The best results are indicated in bold, and the suboptimal results are underlined.

d	F	GPOM	ES	DE	CMA-ES	L SHADE	LES	LGA
30	F1	3.72E-11(3.72E-11)	2.30E+02(1.36E+01)	9.46E+01(1.17E+01)	<u>7.79E-04(8.97E-04)</u>	1.28E-03(7.36E-04)	4.93E+00(4.03E+00)	1.13E+01(5.81E+00)
	F2	4.69E-12(4.69E-12)	2.18E+00(5.24E-01)	1.10E-01(4.35E-03)	<u>8.45E-02(1.64E-02)</u>	1.47E-05(2.12E-06)	1.45E-02(5.21E-03)	1.75E-01(4.80E-02)
	F3	5.57E+01(6.57E+01)	1.41E+03(1.26E+02)	1.02E+03(5.47E+01)	2.47E+03(2.39E+03)	<u>7.12E+01(9.31E+00)</u>	8.10E+02(1.04E+02)	2.82E+02(1.66E+01)
	F4	6.95E+01(6.95E+01)	3.35E+03(6.76E+02)	1.99E+03(5.61E+02)	2.21E+02(1.02E+00)	<u>1.04E+02(4.24E+00)</u>	6.11E+02(1.22E+02)	3.76E+02(3.14E+01)
	F5	3.61E+01(3.61E+01)	5.52E+01(1.45E+01)	1.32E+00(2.70E-01)	0.00E+00(0.00E+00)	<u>0.00E+00(0.00E+00)</u>	1.99E+02(4.46E+01)	0.00E+00(0.00E+00)
	F6	1.69E-09(1.69E-09)	3.97E+02(9.66E+00)	5.29E+02(1.74E+02)	<u>8.99E-02(6.01E-03)</u>	1.54E-01(8.94E-02)	1.11E+01(7.44E+00)	2.25E+01(5.33E+00)
	F7	3.78E-13(3.78E-13)	1.61E+03(5.19E+01)	7.62E+03(9.02E+02)	<u>3.44E+00(7.67E-01)</u>	1.25E+01(6.46E+00)	1.20E+02(3.92E+01)	6.97E+01(2.00E+01)
	F8	6.23E-06(6.23E-06)	4.21E+05(6.85E+04)	3.26E+05(4.66E+04)	<u>3.15E+02(3.90E+02)</u>	3.08E+01(3.53E+00)	3.01E+03(2.28E+03)	1.63E+03(2.94E+02)
	F9	1.60E+02(1.60E+02)	4.44E+05(8.88E+04)	7.06E+05(9.64E+04)	4.17E+01(1.20E+01)	<u>5.85E+01(5.42E+01)</u>	2.37E+03(6.93E+02)	1.38E+03(4.40E+02)
	F10	2.24E+03(2.24E+03)	3.56E+06(1.48E+06)	2.33E+07(6.30E+06)	3.39E+05(1.18E+05)	<u>1.16E+04(5.72E+03)</u>	7.58E+04(2.93E+04)	2.67E+05(5.13E+04)
	F11	7.38E+00(7.38E+00)	1.59E+03(5.31E+02)	5.73E+03(8.62E+02)	5.55E+03(3.21E+03)	<u>1.53E+02(1.13E+02)</u>	2.36E+02(2.59E+01)	3.95E+02(1.40E+02)
	F12	5.13E-04(5.13E-04)	4.18E+09(4.62E+08)	1.37E+10(8.87E+08)	2.91E+11(2.89E+10)	<u>4.10E+05(4.53E+05)</u>	1.04E+08(6.51E+07)	9.59E+07(2.87E+07)
	F13	6.76E-05(6.76E-05)	1.57E+03(6.29E+01)	1.07E+03(8.97E+01)	9.66E+00(1.62E+00)	<u>2.44E+00(1.41E+00)</u>	8.61E+01(3.33E+01)	2.40E+02(3.31E+01)
	F14	2.29E-04(2.29E-04)	9.04E+01(1.08E+01)	5.84E+02(8.93E+01)	1.92E+00(1.14E+00)	<u>4.38E-02(2.39E-02)</u>	6.01E+00(1.54E+00)	4.02E+00(7.88E-01)
	F15	7.84E+01(7.84E+01)	1.62E+03(1.29E+02)	4.31E+03(6.26E+02)	4.27E+04(3.66E+04)	<u>1.16E+02(1.08E+01)</u>	8.73E+02(1.65E+02)	2.84E+02(1.90E+01)
	F16	2.55E+01(2.55E+01)	4.62E+01(4.62E+00)	5.44E+01(5.74E+00)	3.18E+01(3.66E+00)	<u>1.64E+01(5.59E+00)</u>	7.17E+00(9.49E-01)	3.24E+01(8.73E-01)
	F17	2.79E-05(2.79E-05)	2.47E+01(7.36E+00)	2.43E+01(4.93E+00)	<u>3.78E-01(8.36E-02)</u>	4.67E-01(9.78E-02)	9.74E+00(3.39E+00)	2.21E+00(2.95E-01)
	F18	1.30E-01(1.30E-01)	9.84E+01(1.68E+01)	1.19E+02(4.66E+01)	<u>2.26E+00(5.51E-01)</u>	9.34E-01(3.55E-01)	3.43E+01(1.02E+01)	1.21E+01(2.63E+00)
	F19	4.82E+00(4.82E+00)	5.43E+01(4.16E+00)	5.00E+01(1.17E+01)	5.94E+00(4.07E-01)	<u>5.44E+00(4.67E-01)</u>	1.61E+01(2.11E+00)	7.06E+00(2.09E-01)
	F20	-1.32E+01(-1.32E+01)	1.25E+05(3.14E+04)	1.08E+05(2.55E+04)	3.27E+00(1.03E-01)	<u>3.13E+00(9.10E-02)</u>	-2.72E+01(1.03E+01)	9.09E+01(8.60E+01)
	F21	3.36E+01(3.36E+01)	8.80E+01(6.16E-01)	8.56E+01(7.64E-01)	2.89E+00(5.34E-02)	1.44E+01(1.26E+01)	1.99E+01(8.05E+00)	9.98E+00(2.36E+00)
	F22	1.57E+01(1.57E+01)	8.92E+01(1.82E+00)	8.57E+01(6.39E-01)	<u>1.96E+00(5.02E-03)</u>	1.14E+00(7.17E-01)	1.68E+01(3.62E+00)	9.91E+00(4.49E+00)
	F23	3.68E+00(3.68E+00)	1.38E+01(8.94E-01)	1.16E+01(1.80E+00)	<u>3.85E+00(3.62E-01)</u>	3.17E+00(8.65E-01)	3.01E+00(3.26E-01)	4.38E+00(1.13E-01)
	F24	2.81E+02(2.81E+02)	4.10E+04(6.39E+04)	5.32E+04(4.52E+04)	<u>2.23E+02(5.47E+00)</u>	1.72E+02(5.53E+00)	7.08E+02(6.37E+01)	3.69E+02(3.53E+01)
100	F1	5.92E-12(5.92E-12)	1.60E+03(3.45E+01)	4.62E+03(5.31E+02)	4.34E+01(4.29E+00)	1.64E+01(8.78E-01)	2.20E+02(4.07E+01)	1.13E+02(1.69E+01)
	F2	4.70E-12(4.70E-12)	4.08E+01(6.19E+00)	2.24E+01(3.00E+00)	4.17E+01(9.20E+00)	<u>7.58E-02(4.38E-02)</u>	4.56E+00(1.06E+00)	3.28E+00(4.70E-01)
	F3	1.07E-09(1.07E-09)	1.06E+04(7.18E+02)	4.77E+04(2.87E+03)	3.24E+04(8.39E+03)	<u>8.71E+02(9.08E-01)</u>	2.72E+03(1.55E+02)	1.82E+03(4.78E+01)
	F4	1.39E-07(1.39E-07)	6.28E+04(7.31E+03)	2.96E+05(2.45E+04)	3.77E+03(3.11E+02)	<u>1.29E+03(1.69E+02)</u>	5.15E+03(1.02E+03)	2.49E+03(1.23E+02)
	F5	3.04E+02(3.04E+02)	2.03E+01(1.42E+01)	4.64E+00(2.13E+00)	1.63E+02(2.83E+02)	3.98E+00(4.69E+00)	1.30E+03(8.74E+01)	4.05E+00(3.67E+00)
	F6	9.32E-10(9.32E-10)	2.46E+03(2.04E+02)	9.15E+03(2.22E+02)	2.65E+02(1.05E+02)	<u>4.00E+01(5.60E+00)</u>	4.37E+02(4.07E+01)	2.09E+02(9.05E+00)
	F7	2.42E-13(2.42E-13)	1.11E+04(2.21E+03)	6.11E+04(4.18E+03)	2.79E+03(3.55E+02)	<u>1.96E+02(7.71E+01)</u>	1.43E+03(3.21E+02)	9.43E+02(2.72E+02)
	F8	3.01E-08(3.01E-08)	2.09E+07(2.75E+05)	1.60E+08(2.16E+07)	6.06E+04(4.27E+04)	<u>1.35E+04(7.05E+03)</u>	2.40E+05(1.18E+04)	9.43E+04(5.31E+04)
	F9	6.41E+02(6.41E+02)	1.97E+07(1.59E+06)	2.18E+08(2.65E+07)	1.12E+05(8.38E+04)	<u>4.06E+05(9.38E+02)</u>	3.71E+05(1.41E+04)	1.07E+05(2.57E+04)
	F10	2.34E+01(2.34E+01)	5.73E+07(1.15E+07)	3.29E+08(8.13E+07)	7.27E+07(4.91E+07)	<u>4.19E+05(3.99E+04)</u>	2.82E+06(1.01E+06)	3.83E+06(5.67E+05)
	F11	1.71E+01(1.71E+01)	4.63E+03(5.42E+02)	2.41E+04(2.95E+02)	3.25E+04(5.30E+03)	<u>4.59E+02(8.92E+01)</u>	7.82E+02(3.81E+01)	1.27E+03(1.67E+02)
	F12	1.43E-04(1.43E-04)	4.15E+10(1.75E+09)	4.86E+11(8.89E+10)	1.91E+12(5.61E+11)	<u>9.01E+08(4.73E+08)</u>	3.83E+09(2.93E+08)	2.12E+09(1.07E+09)
	F13	7.23E-05(7.23E-05)	4.18E+03(8.22E+01)	6.65E+03(4.61E+02)	6.35E+02(1.15E+02)	<u>3.89E+02(6.17E+01)</u>	1.53E+03(1.03E+02)	9.26E+02(6.39E+01)
	F14	9.07E-05(9.07E-05)	4.51E+02(6.12E+01)	3.85E+03(5.14E+02)	4.15E+02(6.83E+01)	<u>7.45E+00(3.08E+00)</u>	3.57E+01(5.43E+00)	4.11E+01(4.25E+00)
	F15	4.88E+02(4.88E+02)	9.88E+03(7.02E+02)	6.86E+04(8.80E+03)	3.37E+04(1.93E+04)	<u>1.05E+03(9.66E+01)</u>	3.61E+03(2.38E+02)	1.65E+03(1.10E+01)
	F16	4.72E+01(4.72E+01)	8.41E+01(3.87E+00)	1.90E+02(1.40E+01)	5.36E+01(3.48E+00)	<u>3.44E+01(3.21E+00)</u>	1.29E+01(5.22E-01)	5.58E+01(1.36E+00)
	F17	5.50E-07(5.50E-07)	1.26E+03(3.78E+02)	1.77E+04(8.83E+02)	5.71E+00(1.24E+00)	<u>2.61E+00(9.12E-02)</u>	2.10E+01(2.18E+00)	1.20E+01(1.09E+00)
	F18	5.94E-06(5.94E-06)	1.73E+03(1.13E+02)	2.66E+04(3.33E+03)	2.65E+01(4.37E+00)	<u>1.06E+01(1.25E+00)</u>	5.66E+01(9.50E+00)	4.16E+01(4.47E+00)
	F19	6.74E+00(6.74E+00)	5.37E+02(5.46E+01)	5.32E+03(2.05E+03)	1.08E+01(1.71E+00)	<u>8.95E+00(2.98E-01)</u>	2.75E+01(2.74E+00)	1.30E+01(1.12E+00)
	F20	-5.08E+00(-5.08E+00)	1.56E+06(8.58E+04)	5.16E+06(5.28E+05)	3.98E+04(1.36E+04)	<u>1.70E+03(3.56E+02)</u>	4.66E+04(1.65E+04)	2.56E+04(6.50E+03)
	F21	4.03E+01(4.03E+01)	2.10E+02(4.08E+01)	1.22E+03(2.28E+02)	6.56E+01(1.25E+01)	1.37E+01(3.04E+00)	7.62E+01(6.40E-01)	7.35E+01(7.57E-01)
	F22	5.95E+01(5.95E+01)	2.33E+02(1.93E+01)	1.46E+03(4.77E+02)	7.02E+01(2.84E+00)	3.12E+01(1.82E+01)	7.62E+01(4.80E+00)	8.01E+01(6.36E+00)
	F23	4.83E+00(4.83E+00)	1.39E+02(8.62E+00)	1.04E+03(1.59E+02)	5.78E+00(5.92E-01)	<u>5.02E+00(3.81E-01)</u>	5.21E+00(1.55E-01)	7.15E+00(1.37E-01)
	F24	1.24E+03(1.24E+03)	1.32E+07(2.48E+06)	1.30E+08(1.61E+07)	1.61E+03(6.24E+01)	<u>1.24E+03(2.28E+01)</u>	3.52E+03(3.10E+02)	3.37E+03(2.41E+02)
+/-	-	-/-	47/0/1	46/0/2	41/1/6	35/2/11	43/0/5	44/0/4

F.2. BBOB Test With Optimal Solution Disturbed

We further test the performance of the algorithm on the BBOB. Here, the optimal solution of each function is randomly disturbed, that is, $\mathbf{x}^* = \mathbf{x}_{opt} + \mathbf{z}$, where \mathbf{x}^* represents the optimal solution after disturbing, \mathbf{x}_{opt} represents the original optimal solution, \mathbf{x}_{opt} is a vector obtained by random sampling and $\mathbf{z} \in [-1, 1]^d$. The results are displayed in Table 6. We found that the performance of GPOM can still dominate other algorithms when the function optimal solution is disturbed.

Table 6. Additional Experimental results on BBOB ($d = 100$). The best results are indicated in bold, and the suboptimal results are underlined.

F	GPOM	ES	DE	CMA-ES	LSHADE	LES	LGA
F1	1.85E-11(1.85E-11)	2.49E+02(1.29E+01)	6.27E+02(7.89E+01)	5.76E+00(1.69E+00)	2.94E+00(8.22E-01)	2.20E+02(9.01E+00)	8.95E+01(1.19E+01)
F2	3.91E-12(3.91E-12)	5.95E+00(1.05E+00)	4.31E+00(1.50E-01)	6.51E+00(3.23E+00)	1.43E-02(6.93E-03)	3.38E+00(1.48E+00)	3.39E+00(6.19E-01)
F3	9.64E+01(9.64E+01)	2.14E+03(6.76E+01)	4.45E+03(3.99E+02)	1.26E+03(5.32E+01)	5.25E+02(3.82E+01)	2.68E+03(1.15E+02)	1.71E+03(1.32E+02)
F4	6.10E-08(6.10E-08)	3.82E+03(1.69E+02)	1.40E+04(3.22E+03)	1.68E+03(1.23E+02)	7.09E+02(2.40E+01)	5.24E+03(1.18E+03)	2.76E+03(3.12E+02)
F5	3.50E+02(3.50E+02)	7.94E+01(1.34E+01)	2.87E+01(7.49E+00)	2.22E+02(3.84E+02)	3.62E+00(4.75E+00)	1.38E+03(1.12E+01)	5.48E+00(7.74E+00)
F6	2.05E-10(2.05E-10)	4.55E+02(1.58E+01)	1.53E+03(1.66E+02)	5.10E+01(2.66E+01)	7.96E+00(1.51E+00)	3.99E+02(1.13E+01)	2.70E+02(8.24E+01)
F7	3.22E-13(3.22E-13)	1.91E+03(1.57E+02)	8.81E+03(8.16E+02)	7.20E+02(2.23E+02)	4.36E+01(9.36E+00)	1.33E+03(5.42E+02)	8.93E+02(1.21E+02)
F8	1.89E-08(1.89E-08)	5.54E+05(2.29E+04)	4.55E+06(5.34E+05)	3.02E+03(6.65E+02)	8.35E+02(6.27E+01)	3.96E+05(1.21E+05)	2.37E+05(3.39E+04)
F9	6.39E+02(6.39E+02)	5.11E+05(3.79E+04)	4.73E+06(6.75E+05)	4.07E+03(1.11E+03)	7.94E+02(1.25E+02)	3.83E+05(5.75E+04)	9.15E+04(1.63E+04)
F10	1.58E+03(1.58E+03)	9.00E+06(9.13E+05)	4.71E+07(2.44E+06)	1.49E+07(7.37E+06)	6.95E+04(2.16E+04)	2.14E+06(6.53E+05)	3.03E+06(6.19E+05)
F11	2.14E+01(2.14E+01)	7.92E+02(1.49E+02)	3.79E+03(2.36E+02)	5.21E+03(2.43E+02)	7.69E+01(1.13E+01)	7.65E+02(5.37E+01)	1.36E+03(2.93E+02)
F12	1.06E-04(1.06E-04)	3.97E+09(6.42E+07)	2.98E+10(4.86E+08)	1.51E+09(3.66E+08)	6.04E+07(1.93E+07)	3.70E+09(6.08E+08)	2.25E+09(3.85E+08)
F13	5.51E-05(5.51E-05)	1.61E+03(2.89E+01)	2.64E+03(1.44E+02)	2.52E+02(1.45E+01)	1.49E+02(1.06E+01)	1.49E+03(3.60E+01)	1.02E+03(2.22E+02)
F14	5.05E-05(5.05E-05)	5.67E+01(1.52E+00)	4.11E+02(2.83E+01)	5.52E+01(1.26E+01)	1.05E+00(4.57E-01)	3.85E+01(3.60E+00)	4.21E+01(3.73E+00)
F15	5.11E+02(5.11E+02)	2.16E+03(2.43E+01)	6.55E+03(6.17E+02)	1.27E+03(3.28E+01)	6.41E+02(6.21E+01)	3.23E+03(3.14E+02)	1.70E+03(1.76E+02)
F16	4.84E+01(4.84E+01)	5.14E+01(1.67E+00)	7.31E+01(5.97E+00)	5.25E+01(1.70E+00)	3.85E+01(4.42E+00)	1.48E+01(3.28E+00)	5.31E+01(2.25E+00)
F17	5.90E-07(5.90E-07)	9.25E+00(4.82E-01)	1.98E+02(6.26E+01)	2.43E+00(3.89E-01)	1.14E+00(1.70E-01)	1.24E+01(7.44E-01)	1.02E+01(6.05E-01)
F18	7.01E-06(7.01E-06)	3.54E+01(3.01E-01)	3.04E+02(1.64E+02)	9.59E+00(1.51E+00)	3.74E+00(1.00E+00)	6.79E+01(2.00E+01)	3.39E+01(2.04E+00)
F19	7.07E+00(7.07E+00)	2.15E+01(8.02E-01)	1.54E+02(3.80E+01)	8.39E+00(2.80E-01)	7.52E+00(1.58E-01)	3.46E+01(1.48E+00)	1.33E+01(1.28E+00)
F20	-3.43E+00(-3.43E+00)	1.03E+05(9.88E+03)	6.61E+05(3.47E+04)	1.87E+02(1.78E+02)	3.66E+00(3.87E-02)	6.16E+04(1.48E+04)	6.31E+04(7.62E+03)
F21	6.40E+01(6.40E+01)	8.29E+01(1.20E+00)	1.03E+02(6.73E+00)	2.46E+01(2.67E+00)	1.21E+01(2.52E+00)	7.90E+01(1.46E+00)	7.15E+01(7.37E+00)
F22	5.91E+01(5.91E+01)	8.04E+01(2.71E+00)	9.45E+01(3.28E+00)	1.95E+01(3.81E+00)	1.32E+01(2.31E+00)	7.81E+01(5.26E-01)	7.79E+01(6.09E+00)
F23	5.05E+00(5.05E+00)	6.57E+00(3.51E-01)	1.61E+01(5.17E+00)	5.51E+00(2.24E-01)	4.94E+00(1.06E-01)	5.09E+00(3.62E-01)	6.36E+00(5.37E-01)
F24	1.31E+03(1.31E+03)	2.57E+03(2.56E+02)	1.44E+06(1.77E+05)	1.17E+03(7.12E+01)	9.63E+02(1.01E+02)	3.57E+03(1.69E+02)	3.53E+03(1.90E+02)
win/tie/loss	-/-	23/0/1	23/0/1	20/0/4	17/3/4	21/2/1	21/2/1

F.3. Higher-Dimensional BBOB Test

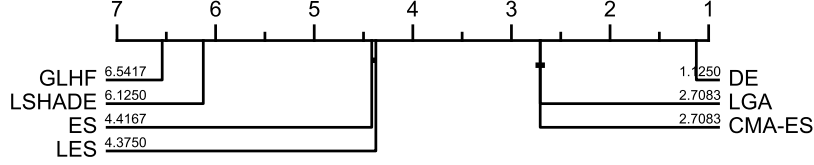


Figure 11. Critical difference diagram of 7 algorithms on 24 BBOB problems with $d = 500$.

Table 7. Additional Experimental results on BBOB ($d = 500$). The best results are indicated in bold, and the suboptimal results are underlined.

F	GPOM	ES	DE	CMA-ES	LSHADE	LES	LGA
F1	1.98E-12(1.98E-12)	2.31E+03(6.40E+01)	6.15E+03(6.55E+02)	2.48E+03(8.03E+01)	<u>1.28E+02(1.87E+01)</u>	2.74E+03(5.65E+01)	4.16E+03(5.26E+01)
F2	2.53E-12(2.53E-12)	9.56E+01(7.06E+00)	2.28E+02(2.16E+01)	2.11E+02(1.23E+01)	<u>1.95E+00(2.56E-01)</u>	7.48E+01(3.45E+00)	9.80E+01(1.12E+01)
F3	2.33E-11(2.33E-11)	1.67E+04(2.48E+02)	5.27E+04(2.96E+03)	3.02E+04(8.66E+02)	<u>3.53E+03(4.12E+02)</u>	1.91E+04(3.75E+02)	2.92E+04(1.15E+03)
F4	2.47E-09(2.47E-09)	5.06E+04(4.80E+03)	2.79E+05(3.05E+04)	8.90E+04(1.14E+04)	<u>6.90E+03(1.38E+03)</u>	1.31E+05(1.28E+04)	1.66E+05(1.40E+04)
F5	4.97E+03(4.97E+03)	3.07E+03(9.94E+01)	3.92E+03(1.36E+02)	1.26E+03(1.95E+02)	<u>2.68E+03(2.48E+02)</u>	8.44E+03(3.08E+02)	2.86E+03(8.51E+01)
F6	8.96E-11(8.96E-11)	3.91E+03(1.55E+02)	9.14E+03(9.31E+01)	4.51E+03(1.07E+02)	<u>2.13E+02(2.23E+01)</u>	3.93E+03(1.58E+02)	5.63E+03(1.75E+02)
F7	1.60E-13(1.60E-13)	1.70E+04(1.91E+02)	5.54E+04(2.24E+03)	2.70E+04(1.34E+03)	<u>8.52E+02(1.20E+02)</u>	2.14E+04(1.58E+03)	2.96E+04(1.03E+03)
F8	3.75E-08(3.75E-08)	2.27E+08(5.75E+06)	1.57E+09(3.05E+07)	2.80E+08(1.56E+07)	<u>8.02E+05(1.97E+05)</u>	1.69E+08(1.41E+07)	4.64E+08(1.05E+07)
F9	3.24E+03(3.24E+03)	2.07E+08(1.80E+07)	1.46E+09(2.76E+08)	2.85E+08(1.61E+07)	<u>5.65E+05(1.21E+05)</u>	2.46E+08(1.50E+07)	6.10E+08(2.26E+07)
F10	2.71E-05(2.71E-05)	1.15E+08(6.37E+06)	4.57E+08(3.63E+07)	2.36E+08(3.43E+07)	<u>2.48E+06(6.76E+05)</u>	9.21E+07(1.18E+07)	9.36E+07(2.24E+07)
F11	1.17E+02(1.17E+02)	4.09E+03(2.27E+02)	1.79E+04(2.97E+03)	2.46E+04(1.39E+03)	<u>1.42E+03(5.16E+02)</u>	4.15E+03(1.31E+02)	5.36E+03(4.49E+02)
F12	2.12E-05(2.12E-05)	4.52E+10(6.07E+08)	1.09E+12(2.33E+11)	2.28E+11(4.24E+10)	<u>1.48E+09(1.87E+08)</u>	4.90E+10(6.16E+08)	1.69E+11(5.93E+09)
F13	1.29E-04(1.29E-04)	4.86E+03(5.22E+01)	7.87E+03(3.62E+02)	4.89E+03(3.96E+01)	<u>1.12E+03(1.31E+01)</u>	5.28E+03(1.04E+02)	6.41E+03(1.02E+02)
F14	1.59E-06(1.59E-06)	2.76E+02(2.14E+01)	1.79E+03(8.21E+01)	6.18E+02(1.89E+01)	<u>1.15E+01(8.01E-01)</u>	2.48E+02(4.01E+01)	5.33E+02(3.10E+01)
F15	1.15E+02(1.15E+02)	1.63E+04(4.57E+02)	5.61E+04(5.73E+02)	2.50E+04(2.12E+03)	<u>4.66E+03(1.29E+02)</u>	2.12E+04(2.15E+03)	2.84E+04(1.07E+03)
F16	6.52E+01(6.52E+01)	6.56E+01(2.66E+00)	8.84E+01(4.04E-01)	7.60E+01(2.29E+00)	<u>5.63E+01(1.15E+00)</u>	2.92E+01(1.06E+00)	7.04E+01(1.29E+00)
F17	2.56E-07(2.56E-07)	8.27E+01(6.17E+00)	3.86E+03(4.66E+02)	4.11E+02(8.71E+01)	<u>1.80E+00(1.06E-01)</u>	1.96E+01(1.30E+00)	1.73E+02(2.50E+01)
F18	2.75E-07(2.75E-07)	1.35E+02(2.64E+01)	3.10E+03(8.03E+02)	3.77E+02(4.29E+01)	<u>7.58E+00(3.17E-01)</u>	7.52E+01(3.07E+00)	2.54E+02(2.65E+01)
F19	8.19E+00(8.19E+00)	1.05E+03(3.85E+01)	7.85E+03(6.28E+02)	1.45E+03(1.78E+02)	<u>1.58E+01(5.79E-01)</u>	1.11E+03(2.97E+01)	2.92E+03(4.50E+01)
F20	-2.65E-01(-2.65E-01)	1.44E+06(5.12E+04)	5.87E+06(4.81E+05)	2.58E+06(1.77E+05)	<u>3.08E+02(8.15E+01)</u>	1.25E+06(5.29E+04)	3.17E+06(9.01E+04)
F21	8.04E+01(8.04E+01)	9.09E+01(8.90E-01)	4.74E+02(7.62E+01)	1.11E+02(8.81E+00)	7.60E+01(7.10E-01)	8.60E+01(3.71E-02)	9.86E+01(1.34E+00)
F22	8.08E+01(8.08E+01)	9.28E+01(3.31E+00)	4.41E+02(4.83E+01)	1.14E+02(8.09E+00)	7.49E+01(2.79E+00)	8.62E+01(7.24E-02)	9.76E+01(1.64E+00)
F23	1.68E+00(1.68E+00)	1.05E+01(2.53E+00)	2.93E+02(3.11E+01)	3.82E+01(1.42E+01)	1.65E+00(6.59E-02)	1.68E+00(2.10E-02)	1.25E+01(1.24E+00)
F24	7.46E+03(7.46E+03)	6.49E+05(1.51E+05)	3.25E+07(4.36E+06)	3.41E+06(6.66E+05)	7.28E+03(7.25E+01)	2.21E+04(6.86E+02)	1.25E+06(1.77E+05)
win/tie/loss	-/-	22/1/1	23/0/1	23/0/1	18/2/4	22/1/1	23/0/1

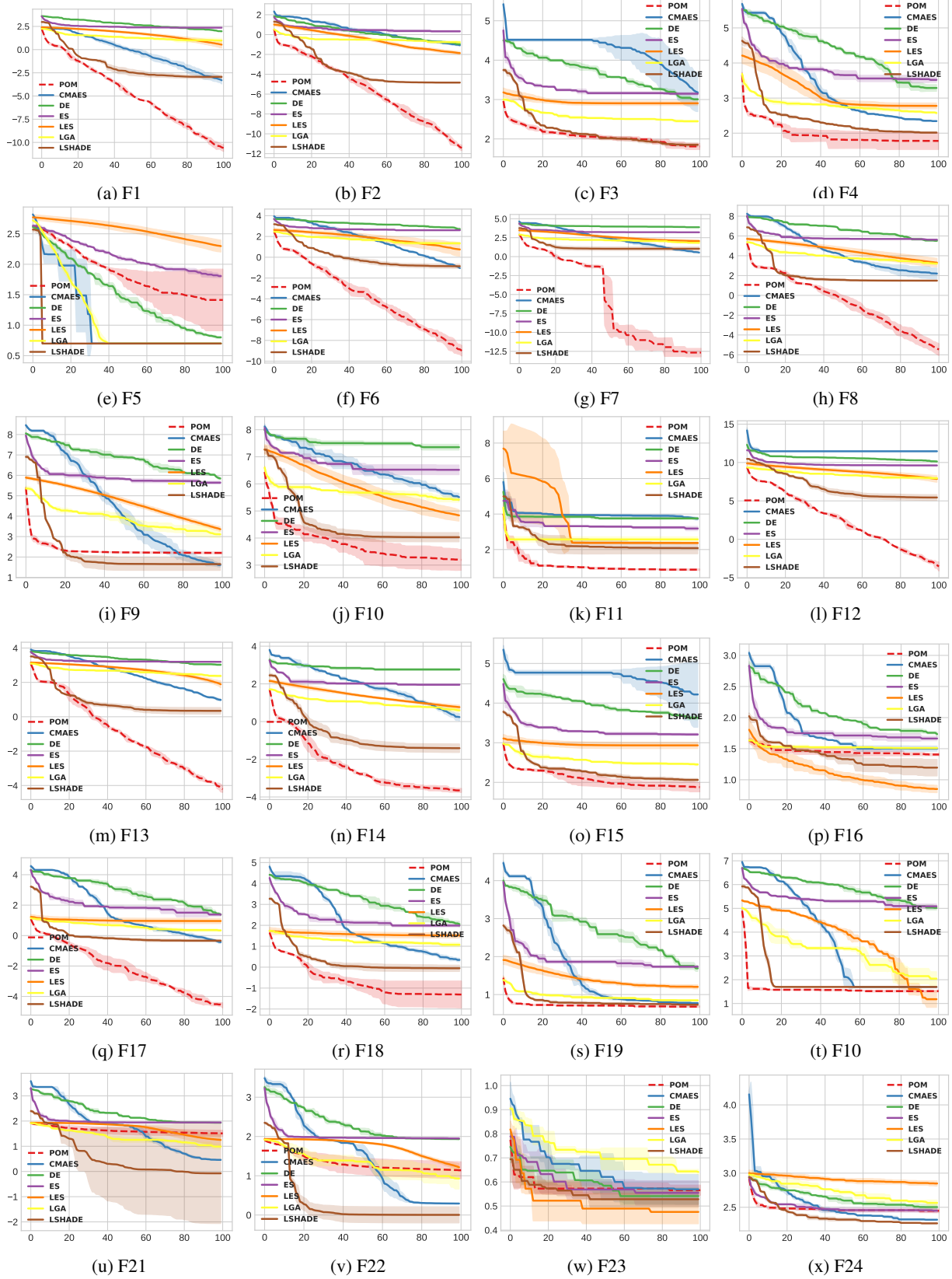


Figure 12. The log convergence curves of GPOM and other baselines. It shows the convergence curve of these algorithms on functions in BBOB with $d = 30$.

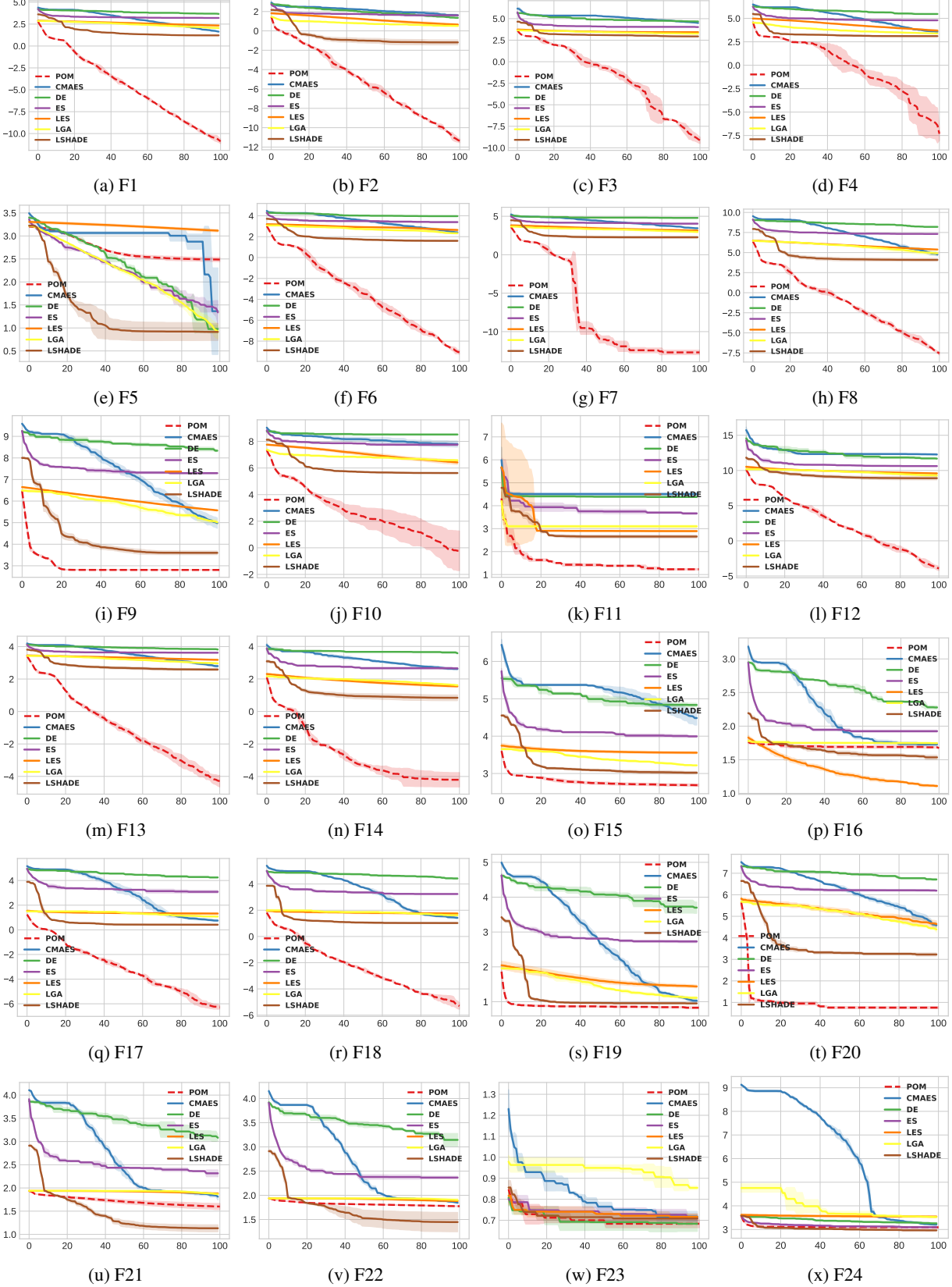


Figure 13. The log convergence curves of GPOM and other baselines. It shows the convergence curve of these algorithms on the functions in BBOB with $d = 100$.

G. Results of Analysis Study

Table 8. Results of ablation experiments. The best results are indicated in bold, and the suboptimal results are underlined. Here $d = 30$.

F	NO LMM	NO LCM	NO MASK	UNTRAINED	GPOM
F1	8.85E+00(8.85E+00)	5.86E-07(5.86E-07)	3.09E+01(3.09E+01)	4.74E-03(4.74E-03)	5.58E-15(5.58E-15)
F2	6.41E-03(6.41E-03)	3.26E-08(3.26E-08)	2.97E-01(2.97E-01)	2.29E-06(2.29E-06)	1.67E-17(1.67E-17)
F3	2.77E+02(2.77E+02)	<u>5.55E+01(5.55E+01)</u>	4.34E+02(4.34E+02)	1.56E+02(1.56E+02)	1.34E+00(1.34E+00)
F4	3.55E+02(3.55E+02)	<u>7.95E+01(7.95E+01)</u>	7.37E+02(7.37E+02)	1.06E+03(1.06E+03)	2.92E+01(2.92E+01)
F5	2.39E+00(2.39E+00)	4.75E+01(4.75E+01)	3.05E+01(3.05E+01)	3.92E+01(3.92E+01)	1.83E+01(1.83E+01)
F6	5.44E+01(5.44E+01)	6.85E-06(6.85E-06)	6.70E+01(6.70E+01)	5.69E-02(5.69E-02)	5.15E-13(5.15E-13)
F7	3.30E+02(3.30E+02)	<u>2.51E+02(2.51E+02)</u>	1.70E+02(1.70E+02)	1.71E+01(1.71E+01)	6.28E-03(6.28E-03)
F8	3.71E+03(3.71E+03)	4.26E+04(4.26E+04)	1.34E+04(1.34E+04)	5.52E+00(5.52E+00)	1.24E-11(1.24E-11)
F9	5.37E+03(5.37E+03)	<u>1.51E+02(1.51E+02)</u>	8.09E+03(8.09E+03)	1.36E+02(1.36E+02)	1.32E+02(1.32E+02)
F10	9.45E+05(9.45E+05)	9.15E+02(9.15E+02)	6.47E+05(6.47E+05)	2.73E+05(2.73E+05)	1.22E+03(1.22E+03)
F11	2.69E+02(2.69E+02)	9.26E+00(9.26E+00)	1.79E+02(1.79E+02)	8.17E+01(8.17E+01)	4.92E+01(4.92E+01)
F12	1.81E+08(1.81E+08)	3.35E-02(3.35E-02)	3.31E+08(3.31E+08)	2.07E+04(2.07E+04)	2.87E-07(2.87E-07)
F13	2.95E+02(2.95E+02)	2.76E-03(2.76E-03)	5.71E+02(5.71E+02)	1.76E+01(1.76E+01)	1.05E-05(1.05E-05)
F14	1.53E+01(1.53E+01)	3.95E-04(3.95E-04)	5.66E+00(5.66E+00)	4.46E-02(4.46E-02)	1.16E-04(1.16E-04)
F15	3.71E+02(3.71E+02)	<u>1.14E+02(1.14E+02)</u>	3.84E+02(3.84E+02)	1.94E+02(1.94E+02)	9.35E+01(9.35E+01)
F16	2.92E+01(2.92E+01)	2.76E+01(2.76E+01)	2.91E+01(2.91E+01)	2.66E+01(2.66E+01)	1.24E+01(1.24E+01)
F17	6.19E+00(6.19E+00)	<u>2.23E+02(2.23E+02)</u>	4.75E+00(4.75E+00)	2.97E-01(2.97E-01)	5.06E-07(5.06E-07)
F18	2.21E+01(2.21E+01)	2.08E+01(2.08E+01)	1.98E+01(1.98E+01)	2.25E+00(2.25E+00)	2.71E-03(2.71E-03)
F19	8.12E+00(8.12E+00)	5.06E+00(5.06E+00)	9.64E+00(9.64E+00)	5.63E+00(5.63E+00)	5.62E+00(5.62E+00)
F20	4.05E+02(4.05E+02)	-2.75E+01(-2.75E+01)	1.56E+03(1.56E+03)	-3.11E+00(-3.11E+00)	-1.84E+01(-1.84E+01)
F21	3.11E+01(3.11E+01)	2.20E+01(2.20E+01)	6.55E+01(6.55E+01)	6.45E+01(6.45E+01)	3.65E+01(3.65E+01)
F22	6.31E+00(6.31E+00)	<u>1.08E+01(1.08E+01)</u>	5.10E+01(5.10E+01)	6.32E+01(6.32E+01)	3.86E+01(3.86E+01)
F23	3.63E+00(3.63E+00)	3.49E+00(3.49E+00)	3.31E+00(3.31E+00)	3.23E+00(3.23E+00)	3.77E+00(3.77E+00)
F24	3.55E+02(3.55E+02)	2.60E+02(2.60E+02)	3.98E+02(3.98E+02)	2.88E+02(2.88E+02)	3.41E+02(3.41E+02)

Table 9. Results of Training Dataset Experiments. The best results are indicated in bold, and the suboptimal results are underlined.

F	8	7	6	5	4	3	2	1
F1	9.86E-08(9.86E-08)	4.15E-11(4.15E-11)	6.99E-09(6.99E-09)	2.06E-10(2.06E-10)	1.37E-13(1.37E-13)	5.61E-12(5.61E-12)	4.23E-13(4.23E-13)	2.36E-01(2.36E-01)
F2	1.87E-08(1.87E-08)	5.26E-13(5.26E-13)	8.51E-11(8.51E-11)	7.17E-12(7.17E-12)	1.59E-15(1.59E-15)	3.88E-14(3.88E-14)	6.82E-15(6.82E-15)	6.21E-10(6.21E-10)
F3	1.28E-01(1.28E-01)	4.11E-01(4.11E-01)	8.69E+00(8.69E+00)	5.75E-01(5.75E-01)	6.26E-01(6.26E-01)	1.93E-10(1.93E-10)	1.99E-01(1.99E-01)	3.79E+02(3.79E+02)
F4	5.67E+01(5.67E+01)	1.22E+00(1.22E+00)	2.20E+02(2.20E+02)	4.74E+00(4.74E+00)	1.80E+00(1.80E+00)	6.85E+01(6.85E+01)	3.96E+00(3.96E+00)	6.21E+02(6.21E+02)
F5	2.61E+02(2.61E+02)	2.57E+02(2.57E+02)	2.59E+02(2.59E+02)	2.40E+02(2.40E+02)	3.14E+02(3.14E+02)	2.85E+02(2.85E+02)	3.07E+02(3.07E+02)	3.85E+02(3.85E+02)
F6	9.51E-07(9.51E-07)	1.33E-09(1.33E-09)	1.95E-07(1.95E-07)	4.78E-09(4.78E-09)	9.30E-12(9.30E-12)	3.68E-10(3.68E-10)	3.07E-11(3.07E-11)	2.07E-01(2.07E-01)
F7	8.87E-14(8.87E-14)	1.11E-13(1.11E-13)	2.39E-13(2.39E-13)	1.08E-12(1.08E-12)	1.67E-13(1.67E-13)	2.90E-13(2.90E-13)	1.50E-13(1.50E-13)	2.85E+00(2.85E+00)
F8	1.33E-05(1.33E-05)	1.28E-07(1.28E-07)	5.65E-05(5.65E-05)	2.68E-07(2.68E-07)	5.90E-10(5.90E-10)	3.03E-07(3.03E-07)	7.11E-09(7.11E-09)	1.03E+02(1.03E+02)
F9	6.38E+02(6.38E+02)	6.36E+02(6.36E+02)	6.38E+02(6.38E+02)	6.37E+02(6.37E+02)	6.38E+02(6.38E+02)	6.35E+02(6.35E+02)	6.39E+02(6.39E+02)	7.07E+02(7.07E+02)
F10	1.46E+03(1.46E+03)	6.10E+01(6.10E+01)	1.30E+04(1.30E+04)	3.84E+03(3.84E+03)	1.44E+03(1.44E+03)	1.16E+03(1.16E+03)	1.51E+03(1.51E+03)	2.11E+04(2.11E+04)
F11	4.65E+02(4.65E+02)	1.29E+02(1.29E+02)	5.38E+02(5.38E+02)	2.72E+02(2.72E+02)	1.67E+02(1.67E+02)	1.58E+02(1.58E+02)	1.61E+02(1.61E+02)	9.73E+01(9.73E+01)
F12	4.94E-04(4.94E-04)	1.43E-04(1.43E-04)	1.32E-01(1.32E-01)	1.61E-04(1.61E-04)	1.45E-06(1.45E-06)	4.48E-04(4.48E-04)	6.44E-06(6.44E-06)	2.02E+04(2.02E+04)
F13	1.48E-03(1.48E-03)	4.61E-04(4.61E-04)	2.26E-02(2.26E-02)	6.23E-04(6.23E-04)	6.64E-05(6.64E-05)	4.17E-04(4.17E-04)	1.57E-04(1.57E-04)	3.79E+01(3.79E+01)
F14	1.05E-04(1.05E-04)	1.51E-04(1.51E-04)	2.25E-04(2.25E-04)	8.33E-05(8.33E-05)	1.99E-05(1.99E-05)	1.35E-04(1.35E-04)	1.50E-05(1.50E-05)	7.15E-02(7.15E-02)
F15	5.65E+02(5.65E+02)	5.55E+02(5.55E+02)	5.69E+02(5.69E+02)	5.51E+02(5.51E+02)	3.96E+02(3.96E+02)	5.62E+02(5.62E+02)	5.27E+02(5.27E+02)	7.27E+02(7.27E+02)
F16	2.98E+01(2.98E+01)	3.39E+01(3.39E+01)	3.25E+01(3.25E+01)	2.68E+01(2.68E+01)	2.71E+01(2.71E+01)	2.88E+01(2.88E+01)	2.91E+01(2.91E+01)	3.99E+01(3.99E+01)
F17	1.80E-04(1.80E-04)	6.23E-06(6.23E-06)	1.94E-04(1.94E-04)	1.35E-05(1.35E-05)	3.49E-07(3.49E-07)	1.38E-06(1.38E-06)	5.72E-07(5.72E-07)	2.35E-02(2.35E-02)
F18	4.89E-04(4.89E-04)	3.23E-05(3.23E-05)	1.56E-03(1.56E-03)	4.58E-05(4.58E-05)	1.14E-06(1.14E-06)	2.32E-05(2.32E-05)	4.80E-06(4.80E-06)	4.35E-01(4.35E-01)
F19	7.60E+00(7.60E+00)	7.28E+00(7.28E+00)	7.45E+00(7.45E+00)	7.48E+00(7.48E+00)	7.43E+00(7.43E+00)	7.47E+00(7.47E+00)	7.30E+00(7.30E+00)	8.14E+00(8.14E+00)
F20	-1.37E+01(-1.37E+01)	-5.10E+00(-5.10E+00)	-1.20E+01(-1.20E+01)	-9.09E+00(-9.09E+00)	-7.39E+00(-7.39E+00)	-8.39E+00(-8.39E+00)	-6.46E+00(-6.46E+00)	-6.56E+00(-6.56E+00)
F21	5.96E+01(5.96E+01)	6.45E+01(6.45E+01)	5.89E+01(5.89E+01)	5.58E+01(5.58E+01)	6.04E+01(6.04E+01)	6.70E+01(6.70E+01)	6.42E+01(6.42E+01)	7.08E+01(7.08E+01)
F22	7.47E+01(7.47E+01)	7.67E+01(7.67E+01)	7.36E+01(7.36E+01)	7.36E+01(7.36E+01)	7.51E+01(7.51E+01)	7.80E+01(7.80E+01)	7.59E+01(7.59E+01)	7.86E+01(7.86E+01)
F23	5.27E+00(5.27E+00)	5.04E+00(5.04E+00)	5.29E+00(5.29E+00)	5.13E+00(5.13E+00)	4.83E+00(4.83E+00)	5.14E+00(5.14E+00)	5.15E+00(5.15E+00)	5.32E+00(5.32E+00)
F24	1.38E+03(1.38E+03)	1.37E+03(1.37E+03)	1.36E+03(1.36E+03)	1.35E+03(1.35E+03)	1.37E+03(1.37E+03)	1.38E+03(1.38E+03)	1.37E+03(1.37E+03)	1.35E+03(1.35E+03)

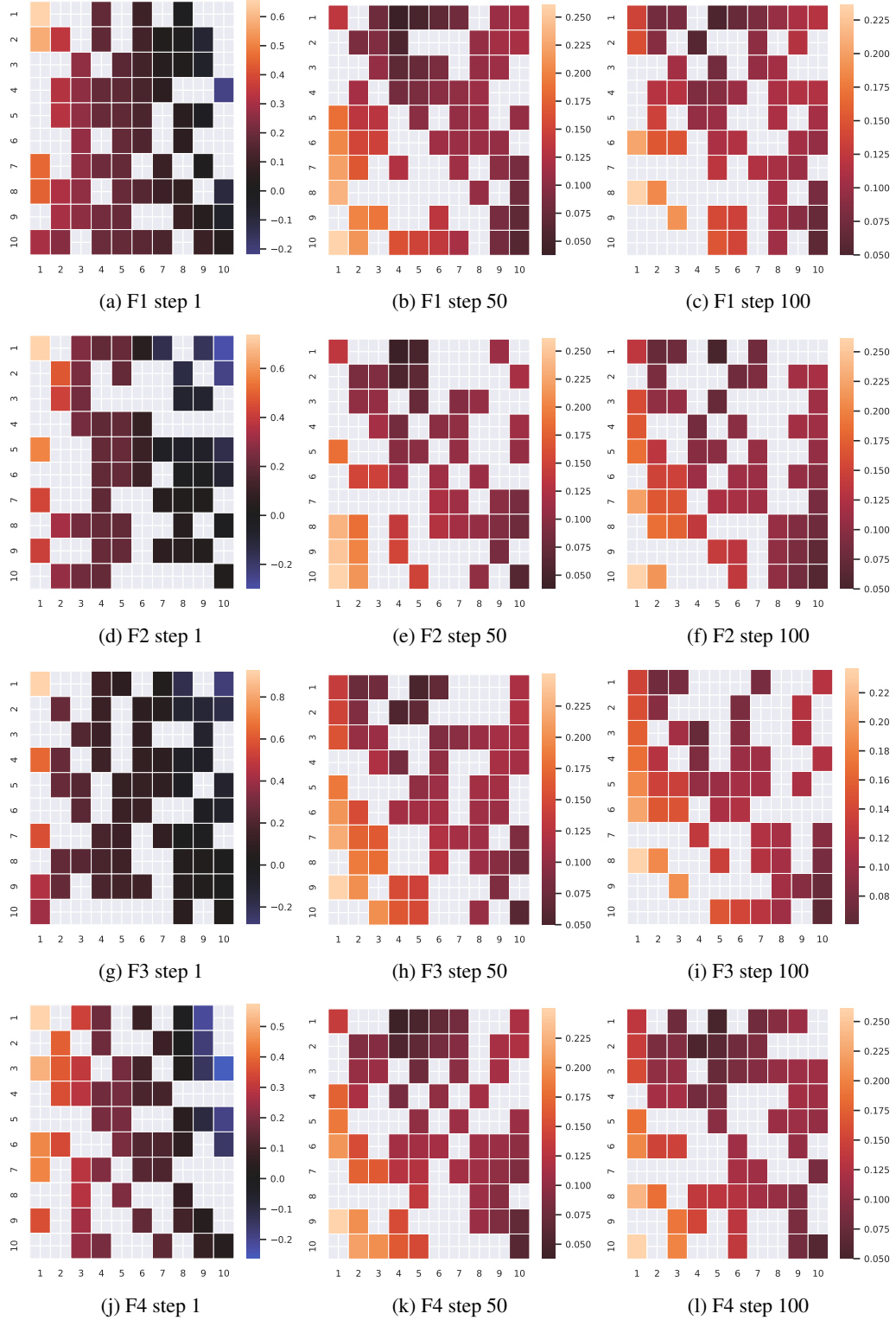


Figure 14. Visualized results of mutation strategy S^t on BBOB (F1-F4) with $d = 100$. Here, $n = 10$ for the sake of clarity. The blank squares in the matrix indicate the masked parts in Eq. (11). Steps 1, 50 and 100 correspond to the 1st, 50th and 100th generations in the population evolution process. The horizontal and vertical axes show the ranking of individuals, with 1 being the best and 10 being the worst in the population. Each row represents the weight assigned to other individuals when performing mutation operations for the corresponding individual.

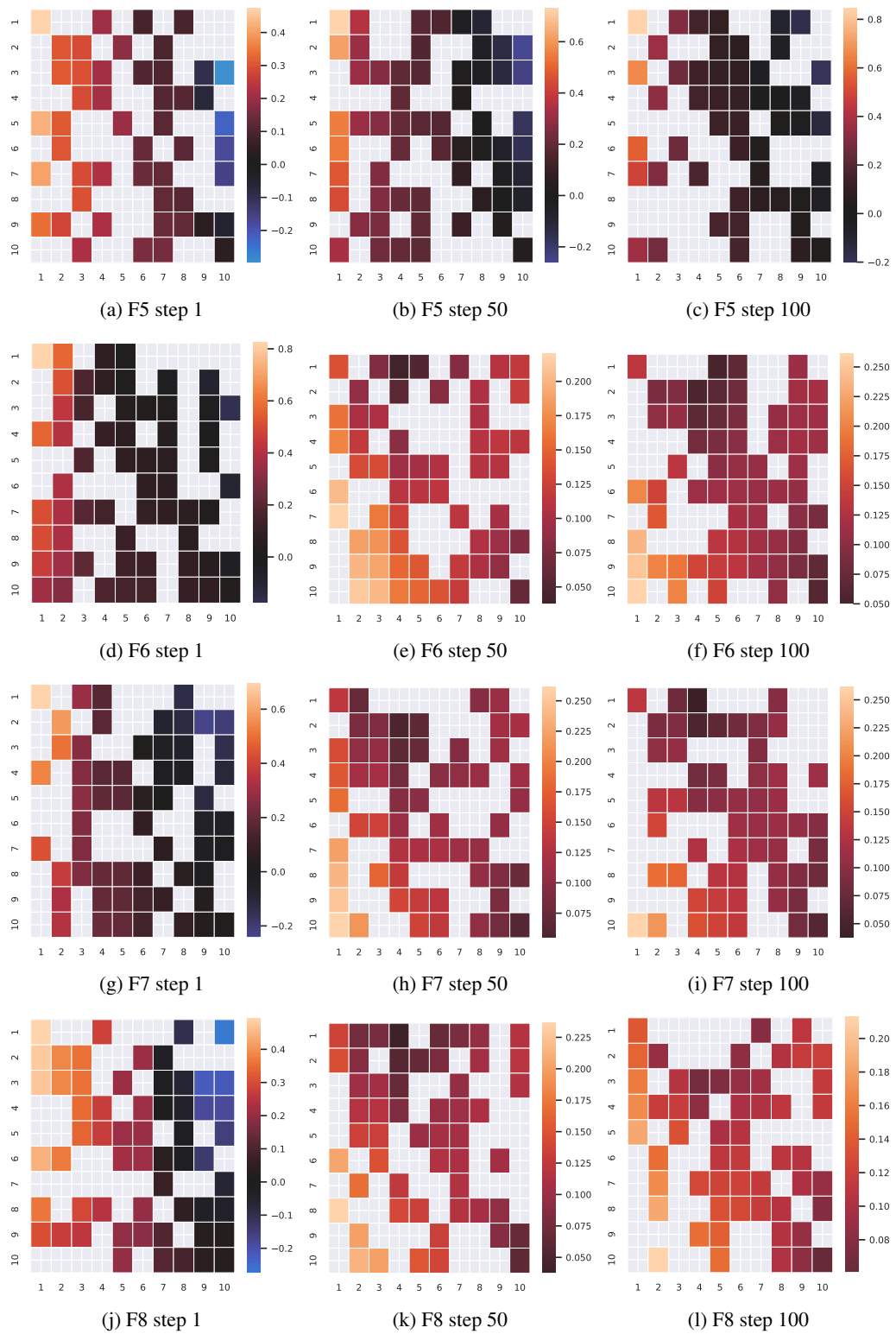


Figure 15. Visualized results of mutation strategy S^t on BBOB (F5-F8) with $d = 100$.

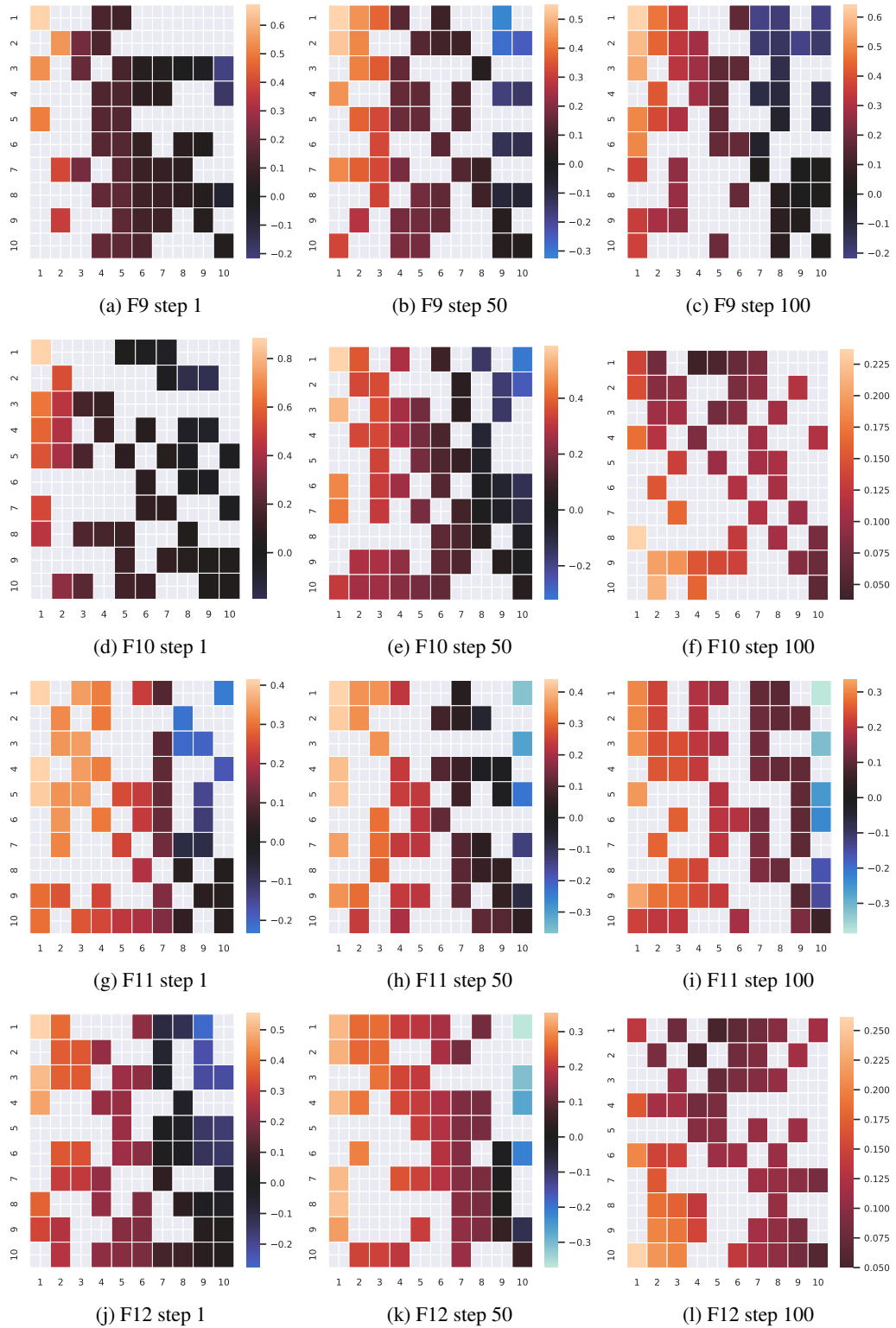


Figure 16. Visualized results of mutation strategy S^t on BBOB (F9-F12) with $d = 100$.

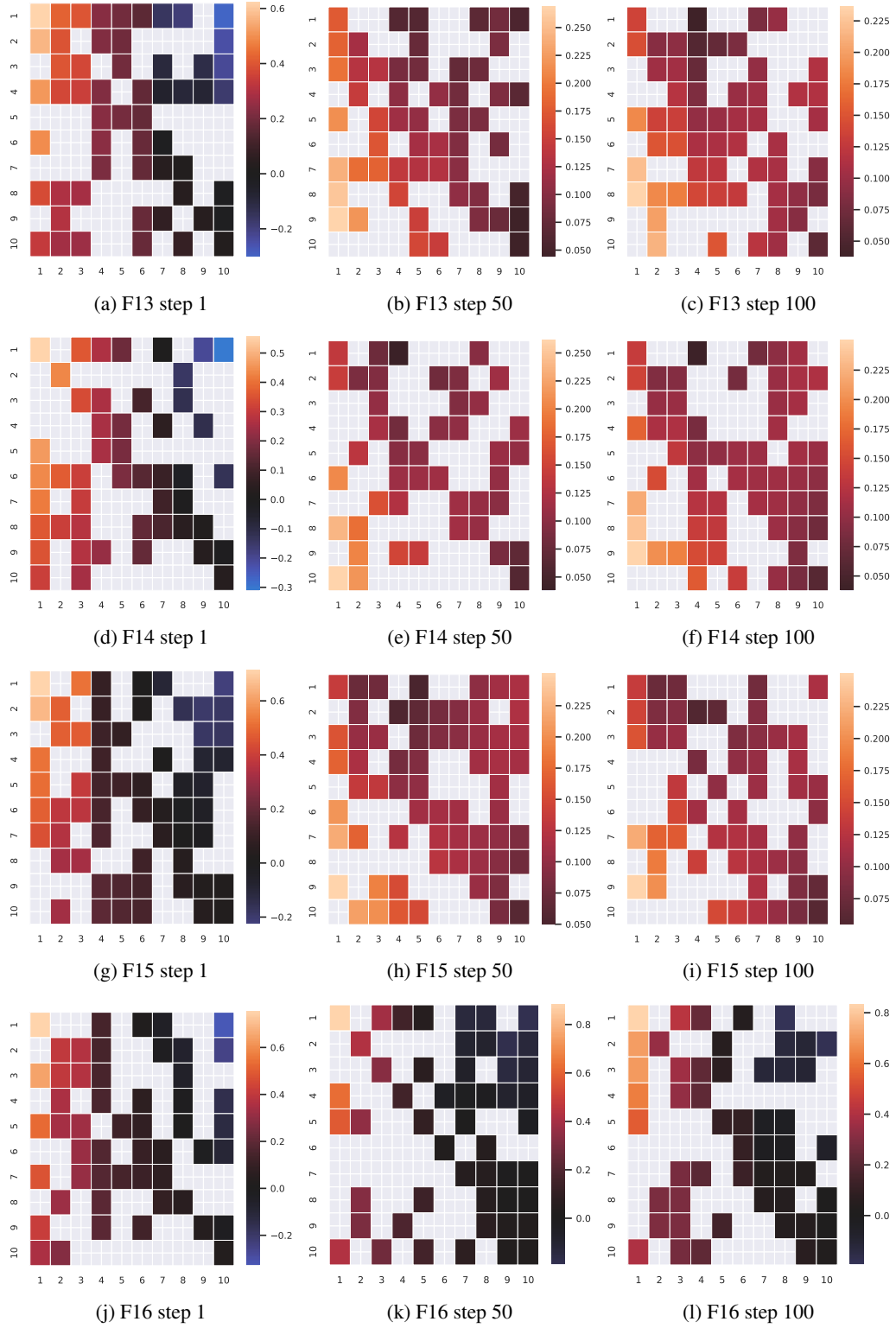


Figure 17. Visualized results of mutation strategy S^t on BBOB (F13-F16) with $d = 100$.

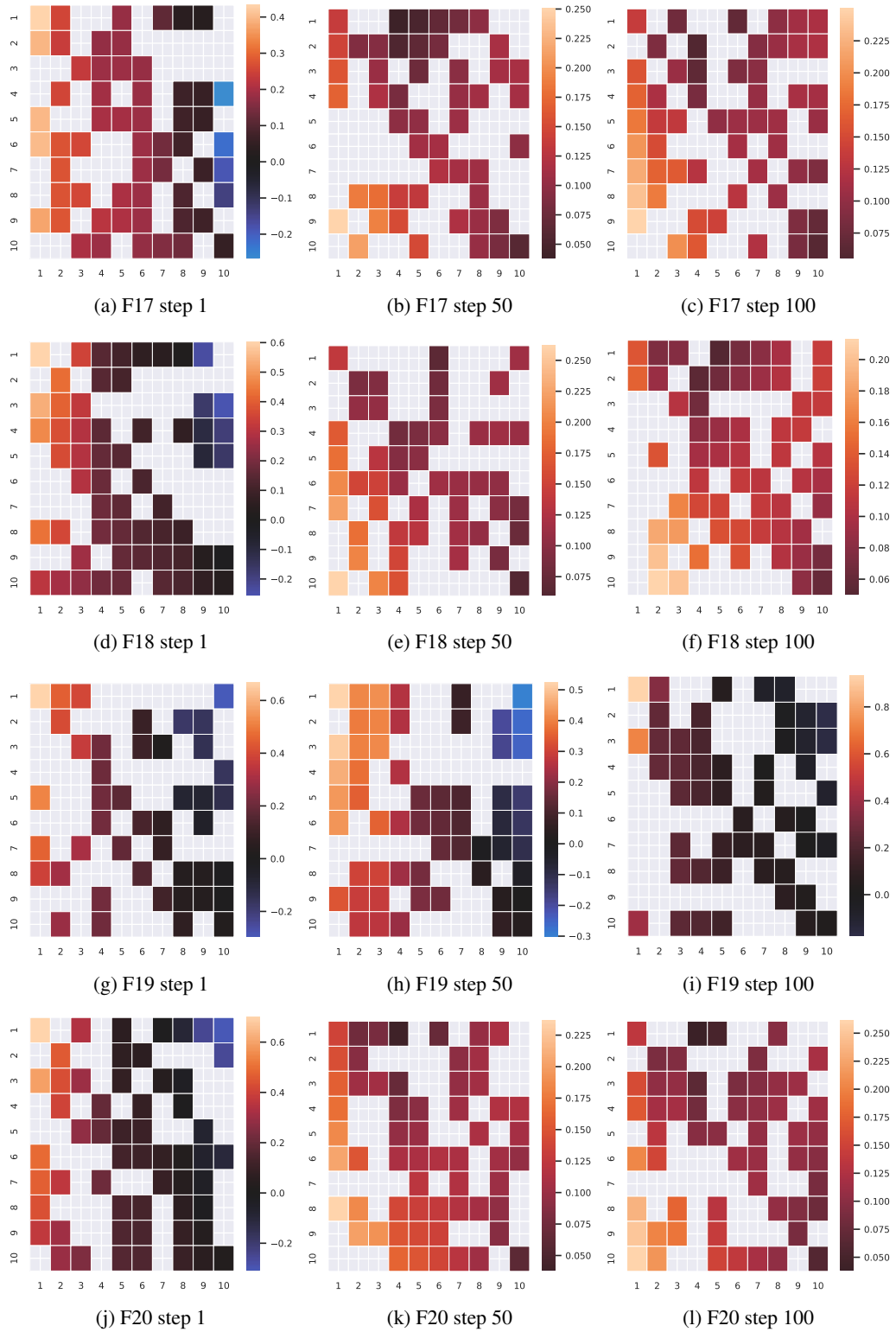

 Figure 18. Visualized results of mutation strategy S^t on BBOB (F17-F20) with $d = 100$.



Figure 19. Visualized results of mutation strategy S^t on BBOB (F21-F24) with $d = 100$.

Table 10. Results of GPOMs of different sizes on BBOB tests ($d = 100$). The best results are indicated in bold, and the suboptimal results are underlined.

F	XS	S	M	L	VL	XL
F1	3.89E-16(3.89E-16)	5.38E-07(5.38E-07)	6.06E-19(6.06E-19)	<u>7.88E-24(7.88E-24)</u>	1.97E-19(1.97E-19)	4.99E-27(4.99E-27)
F2	<u>7.66E-18(7.66E-18)</u>	9.97E-09(9.97E-09)	2.43E-21(2.43E-21)	6.96E-30(6.96E-30)	1.04E-21(1.04E-21)	2.58E-29(2.58E-29)
F3	3.11E-16(3.11E-16)	4.60E+02(4.60E+02)	1.39E-17(1.39E-17)	2.89E-16(2.89E-16)	4.17E+02(4.17E+02)	3.34E-26(3.34E-26)
F4	8.49E-03(8.49E-03)	5.26E+02(5.26E+02)	2.46E-02(2.46E-02)	8.56E-01(8.56E-01)	3.10E+02(3.10E+02)	6.15E-23(6.15E-23)
F5	<u>4.00E+02(4.00E+02)</u>	3.22E+02(3.22E+02)	3.89E+02(3.89E+02)	0.00E+00(0.00E+00)	4.05E+02(4.05E+02)	2.56E+02(2.56E+02)
F6	2.94E-14(2.94E-14)	8.11E-06(8.11E-06)	1.58E-16(1.58E-16)	<u>1.67E-19(1.67E-19)</u>	6.81E-17(6.81E-17)	3.92E-24(3.92E-24)
F7	1.83E-14(1.83E-14)	4.03E-13(4.03E-13)	9.48E-14(9.48E-14)	2.22E-13(2.22E-13)	6.61E-14(6.61E-14)	9.54E-14(9.54E-14)
F8	0.00E+00(0.00E+00)	6.76E-04(6.76E-04)	0.00E+00(0.00E+00)	0.00E+00(0.00E+00)	0.00E+00(0.00E+00)	0.00E+00(0.00E+00)
F9	<u>6.32E+02(6.32E+02)</u>	6.42E+02(6.42E+02)	6.37E+02(6.37E+02)	6.27E+02(6.27E+02)	6.38E+02(6.38E+02)	6.38E+02(6.38E+02)
F10	<u>6.86E-01(6.86E-01)</u>	8.96E+02(8.96E+02)	9.37E+01(9.37E+01)	1.89E+04(1.89E+04)	1.26E+00(1.26E+00)	2.45E-02(2.45E-02)
F11	2.93E+01(2.93E+01)	1.34E+02(1.34E+02)	8.50E+01(8.50E+01)	6.84E+01(6.84E+01)	4.56E+01(4.56E+01)	1.10E+01(1.10E+01)
F12	<u>2.84E-11(2.84E-11)</u>	2.90E+00(2.90E+00)	6.53E-11(6.53E-11)	1.02E-03(1.02E-03)	2.11E-09(2.11E-09)	3.89E-20(3.89E-20)
F13	1.17E-07(1.17E-07)	3.47E-02(3.47E-02)	1.95E-07(1.95E-07)	1.29E-05(1.29E-05)	1.67E-06(1.67E-06)	1.08E-11(1.08E-11)
F14	2.85E-05(2.85E-05)	1.97E-04(1.97E-04)	<u>1.71E-05(1.71E-05)</u>	8.94E-05(8.94E-05)	1.00E-04(1.00E-04)	6.58E-06(6.58E-06)
F15	9.76E+01(9.76E+01)	5.18E+02(5.18E+02)	3.22E+02(3.22E+02)	5.57E+02(5.57E+02)	4.95E+02(4.95E+02)	1.27E-07(1.27E-07)
F16	3.45E+01(3.45E+01)	4.51E+01(4.51E+01)	2.65E+01(2.65E+01)	3.34E+01(3.34E+01)	3.13E+01(3.13E+01)	3.50E+01(3.50E+01)
F17	1.63E-08(1.63E-08)	1.15E-03(1.15E-03)	5.86E-10(5.86E-10)	6.79E-11(6.79E-11)	6.60E-10(6.60E-10)	1.61E-14(1.61E-14)
F18	3.12E-08(3.12E-08)	5.33E-03(5.33E-03)	5.16E-09(5.16E-09)	4.85E-08(4.85E-08)	1.61E-08(1.61E-08)	5.50E-14(5.50E-14)
F19	<u>6.22E+00(6.22E+00)</u>	7.26E+00(7.26E+00)	6.59E+00(6.59E+00)	7.06E+00(7.06E+00)	7.34E+00(7.34E+00)	6.21E+00(6.21E+00)
F20	-5.39E+00(-5.39E+00)	<u>-7.19E+00(-7.19E+00)</u>	-7.71E+00(-7.71E+00)	9.90E-01(9.90E-01)	-4.40E+00(-4.40E+00)	-1.94E+00(-1.94E+00)
F21	5.24E+01(5.24E+01)	6.86E+01(6.86E+01)	5.46E+01(5.46E+01)	2.22E+01(2.22E+01)	6.43E+01(6.43E+01)	4.88E+01(4.88E+01)
F22	7.24E+01(7.24E+01)	7.70E+01(7.70E+01)	7.30E+01(7.30E+01)	6.73E+01(6.73E+01)	7.65E+01(7.65E+01)	7.34E+01(7.34E+01)
F23	5.06E+00(5.06E+00)	5.17E+00(5.17E+00)	5.15E+00(5.15E+00)	5.17E+00(5.17E+00)	5.42E+00(5.42E+00)	5.04E+00(5.04E+00)
F24	1.31E+03(1.31E+03)	1.37E+03(1.37E+03)	<u>1.31E+03(1.31E+03)</u>	1.32E+03(1.32E+03)	1.35E+03(1.35E+03)	1.34E+03(1.34E+03)

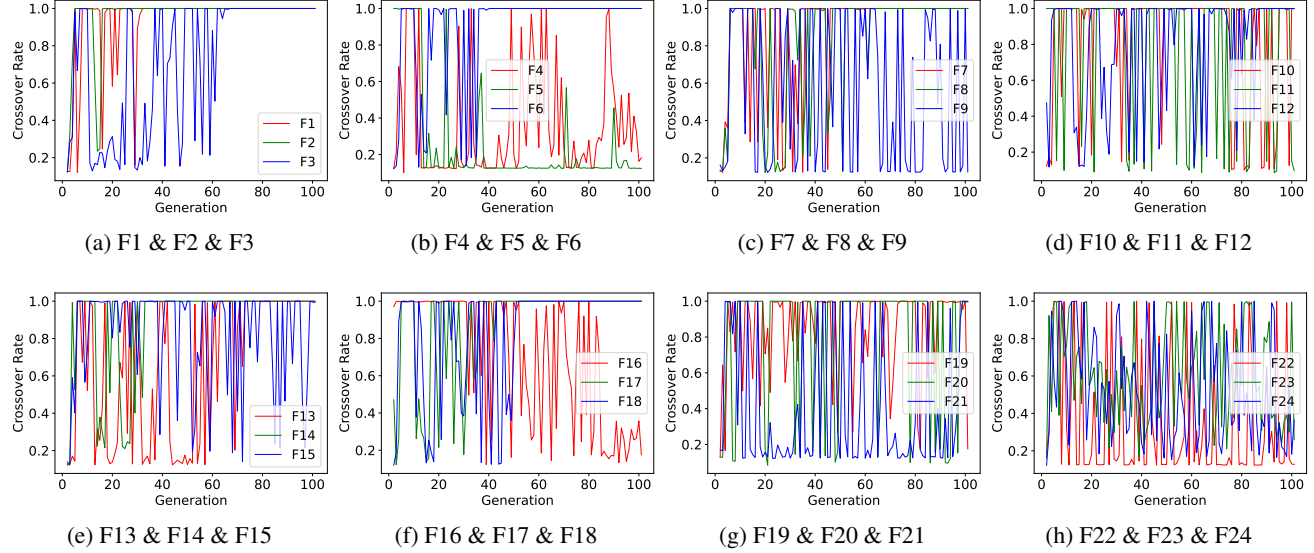


Figure 20. Results of a visual analysis of LCM on BBOB with $d = 100$. Here, $n = 100$. This is the crossover strategy of the individual ranked No. 1. Rank denotes the ranking of an individual. A subgraph illustrates the change in the probability of an individual crossing three tasks as the population evolves.

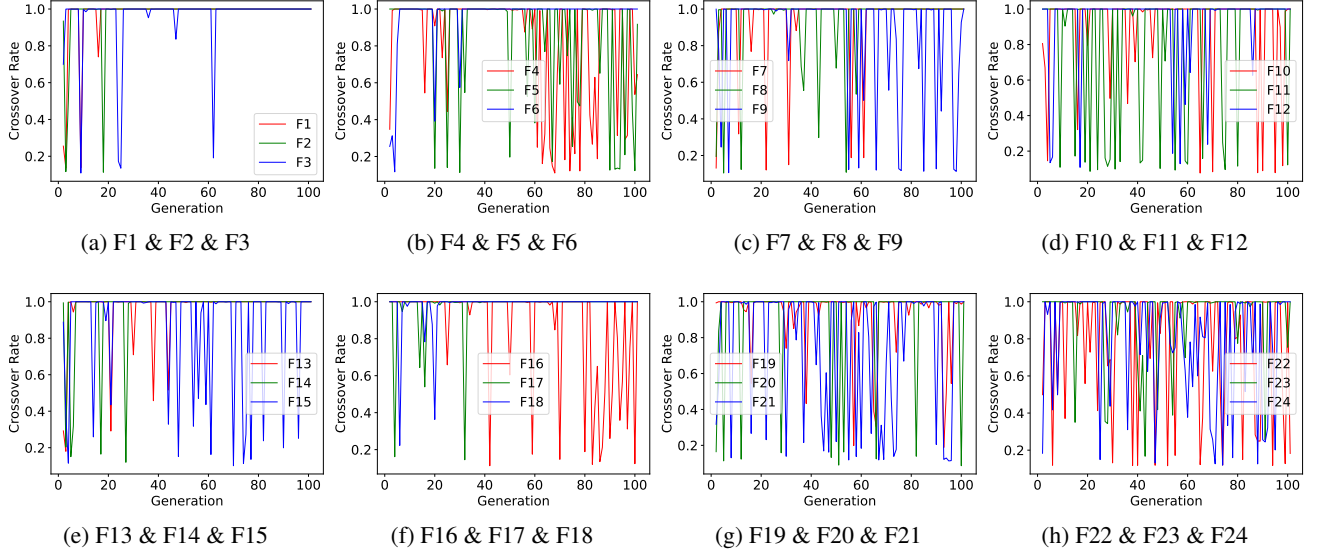


Figure 21. Results of a visual analysis of LCM on BBOB with $d = 100$. Here, $n = 100$. This is the crossover strategy of the individual ranked No. 5. Rank denotes the ranking of an individual. A subgraph illustrates the change in the probability of an individual crossing three tasks as the population evolves.

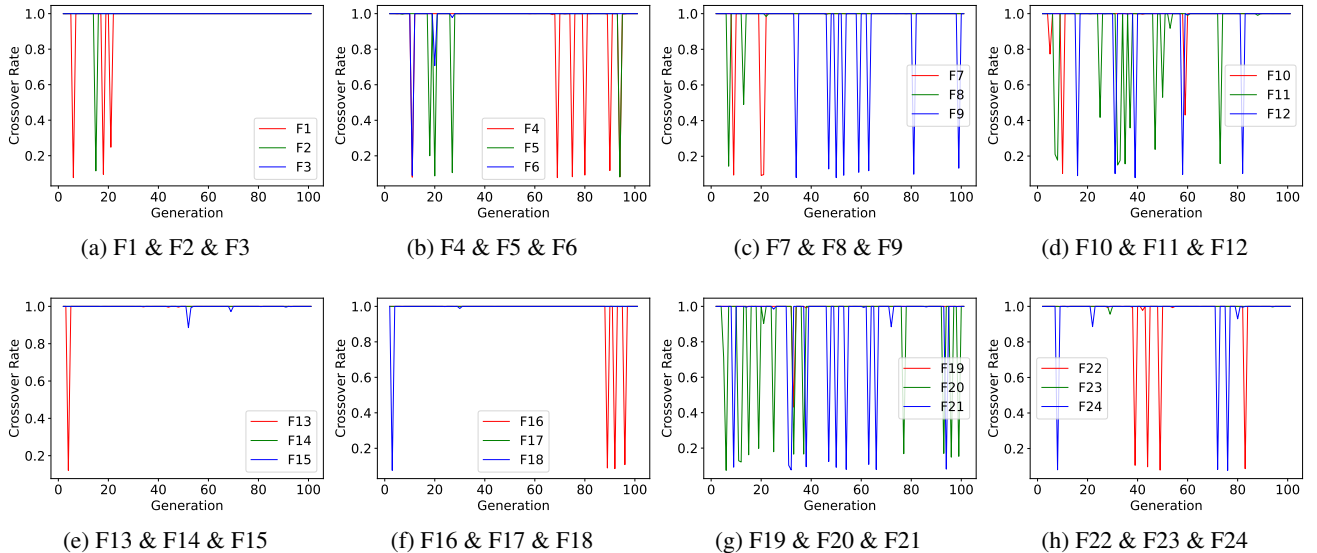


Figure 22. Results of a visual analysis of LCM on BBOB with $d = 100$. Here, $n = 100$. This is the crossover strategy of the individual ranked No. 18. Rank denotes the ranking of an individual. A subgraph illustrates the change in the probability of an individual crossing three tasks as the population evolves.

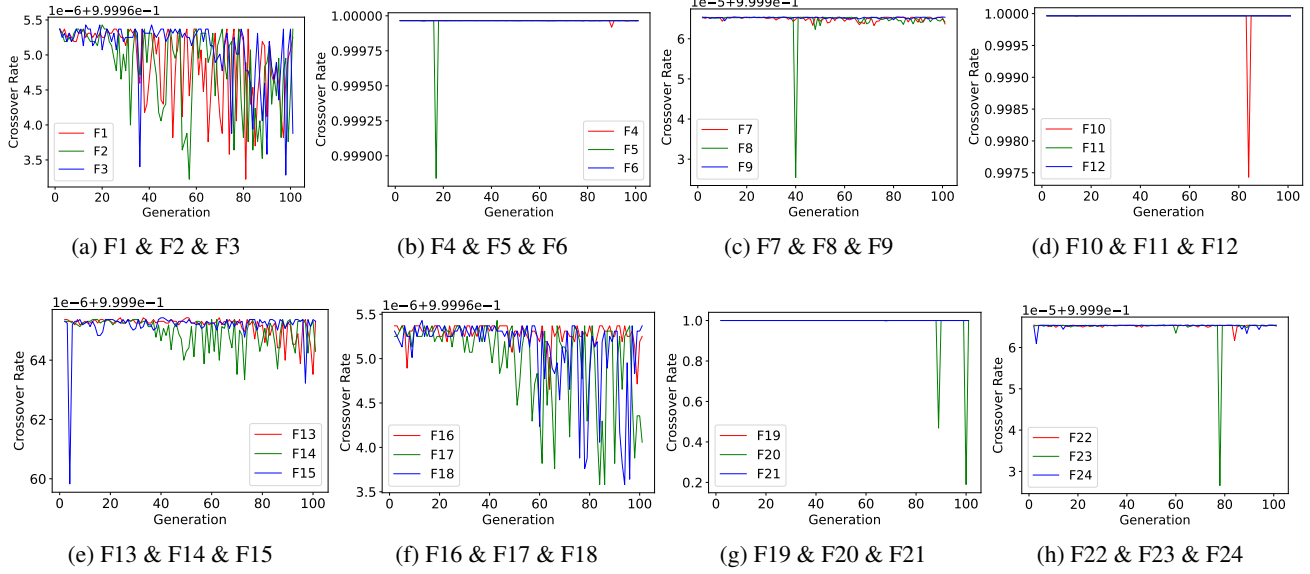


Figure 23. Results of a visual analysis of LCM on BBOB with $d = 100$. Here, $n = 100$. This is the crossover strategy of the individual ranked No. 51. Rank denotes the ranking of an individual. A subgraph illustrates the change in the probability of an individual crossing three tasks as the population evolves.

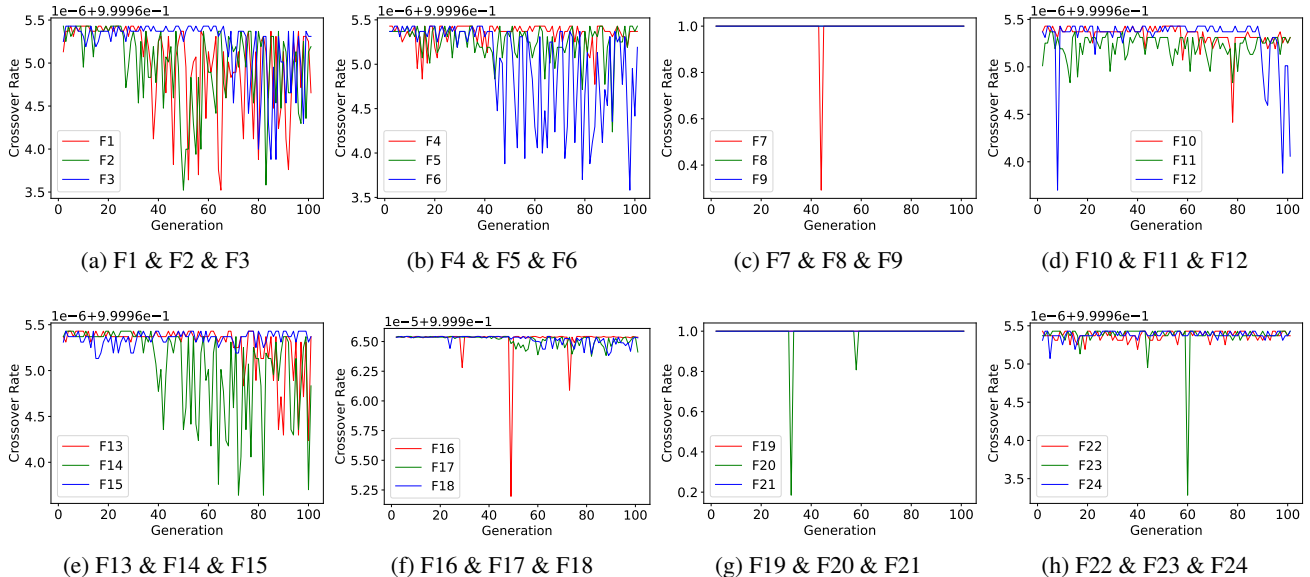


Figure 24. Results of a visual analysis of LCM on BBOB with $d = 100$. Here, $n = 100$. This is the crossover strategy of the individual ranked No. 75. Rank denotes the ranking of an individual. A subgraph illustrates the change in the probability of an individual crossing three tasks as the population evolves.

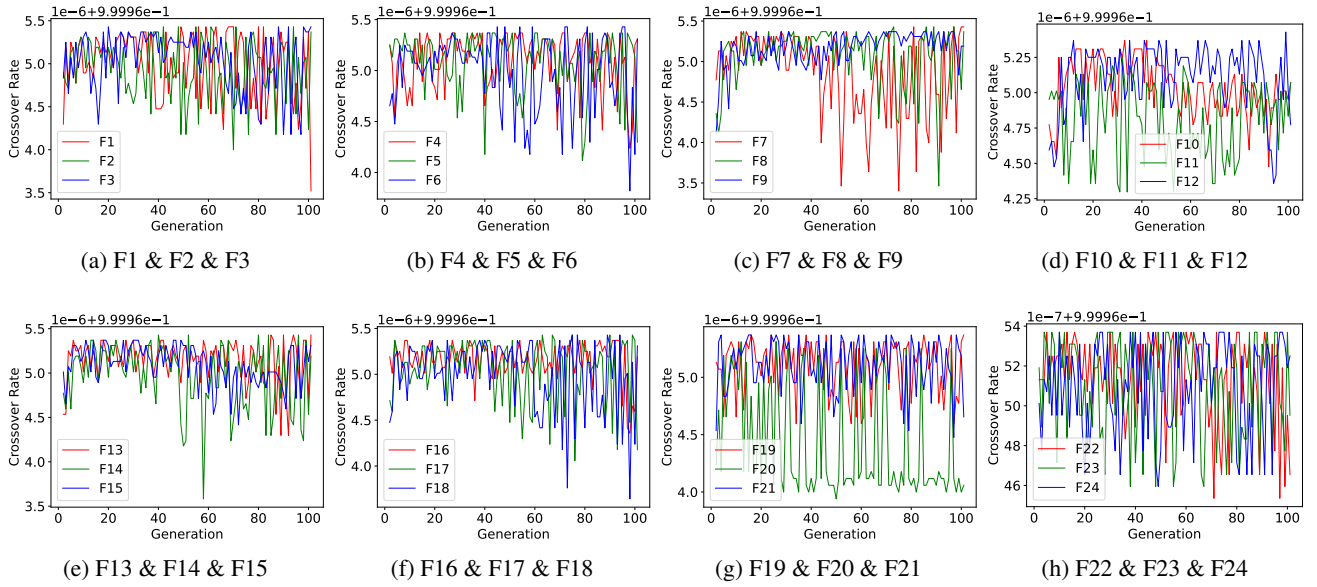


Figure 25. Results of a visual analysis of LCM on BBOB with $d = 100$. Here, $n = 100$. This is the crossover strategy of the individual ranked No. 100. Rank denotes the ranking of an individual. A subgraph illustrates the change in the probability of an individual crossing three tasks as the population evolves.